This article is made available via the ACS COVID-19 subset for unrestricted RESEARCH re-use and analyses in any form or by any means with acknowledgement of the original source. These permissions are granted for the duration of the World Health Organization (WHO) declaration of COVID-19 as a global pandemic.

ACSNANO

www.acsnano.org

Article

Enzyme-Catalyzed One-Step Synthesis of Ionizable Cationic Lipids for Lipid Nanoparticle-Based mRNA COVID-19 Vaccines

Zhongyu Li, Xue-Qing Zhang,* William Ho, Fengqiao Li, Mingzhu Gao, Xin Bai, and Xiaoyang Xu*

Cite This: *ACS Nano* 2022, 16, 18936−18950

Read Online

ACCESS | Metrics & More | Article Recommendations | * Supporting Information

ABSTRACT: Ionizable cationic lipid-containing lipid nanoparticles (LNPs) are the most clinically advanced non-viral gene delivery platforms, holding great potential for gene therapeutics. This is exemplified by the two COVID-19 vaccines employing mRNA-LNP technology from Pfizer/BioNTech and Moderna. Herein, we develop a chemical library of ionizable cationic lipids through a one-step chemical-biological enzyme-catalyzed esterification method, and the synthesized ionizable lipids were further prepared to be LNPs for mRNA delivery. Through orthogonal design of experiment methodology screening, the top-performing AA3-DLin LNPs show outstanding mRNA delivery eficacy and long-term storage capability. Furthermore, the AA3-DLin LNP COVID-19 vaccines encapsulating SARS-CoV-2 spike mRNAs successfully induced strong immunogenicity in a BALB/c mouse model demonstrated by the antibody titers, virus challenge, and T cell immune response studies. The developed AA3-DLin LNPs are an excellent mRNA delivery platform, and this study provides an overall perspective of the ionizable cationic lipids, from aspects of lipid design, synthesis, screening, optimization, fabrication, characterization, and application.

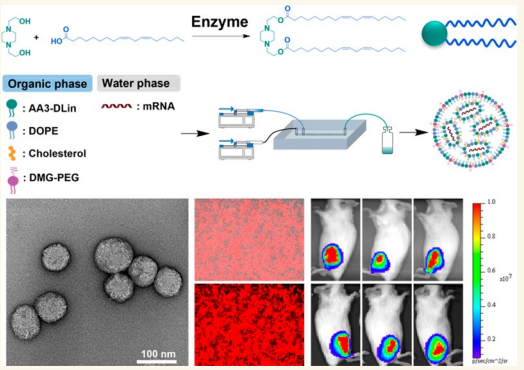

KEYWORDS: *ionizable lipids, lipid nanoparticle, gene delivery, COVID-19 vaccines, mRNA therapeutics*

Coronavirus disease (COVID-19), caused by severe acute respiratory syndrome coronavirus 2 (SARS-CoV-2), was a global catastrophe for public health and resulted in millions of deaths over the past two years. In response, COVID-19 vaccines were developed for preventing the spread of coronavirus, diminishing symptoms of the disease, and saving lives. The most effective COVID-19 vaccines were developed by Pfizer-BioNTech[1] and Moderna[2] using mRNA lipid nanoparticle (mRNA-LNP) technology, and their success truly solidifies the significant impact of mRNA-LNP therapy as a groundbreaking technology in human public health.[3] This provides enormous avenues for mRNA-LNP gene therapy platforms to treat diseases by expressing antigenic or therapeutic proteins.[4] LNPs are the most clinically advanced non-viral based gene delivery vectors for RNAs and overcome the major barrier preventing the development of genetic therapy.[5−8] In general, the FDA-approved LNP formulations contain ionizable cationic lipids, cholesterol, phospholipids, and PEGylated lipids, each with specialized functions indispensable to RNA delivery.[3−6,9] It is worthwhile to note that the ionizable cationic lipid is the most essential material, specifically because it determines the mRNA transfection eficacy and by extension the therapeutic effects.[4−6] Ionizable cationic lipids with acid dissociation constant (pK_a) less than 7 are developed to be protonated at acidic pH environment, and the positive charges can condense negatively charged mRNA via electrostatic interactions while simultaneously promoting self-assembly to encapsulate mRNA, forming LNPs.[4−6,9] This characteristic allows these lipids to be neutrally charged at physiological conditions, improving stability and preventing systemic toxicity.[8−11] Once taken up by the cells, the LNPs are again positively charged in the acidic endosomal environment, which destabilizes the ionic endosomal membrane, facilitating the cytosolic release of mRNA for protein translation.[9] Ionizable cationic lipid mediated mRNA-LNP delivery platforms have exhibited great potential in the field of nanoparticle-mediated vaccines,[1,2] gene editing,[12−14] and cancer therapy.[15,16] Consequently, to fully realize the effectiveness of

Received: August 5, 2022
Accepted: October 14, 2022
Published: October 21, 2022

Downloaded via NEW JERSEY INST OF TECHNOLOGY on April 30, 2023 at 06:25:18 (UTC).
See https://pubs.acs.org/sharingguidelines for options on how to legitimately share published articles.

ACS Publications

© 2022 American Chemical Society

https://doi.org/10.1021/acsnano.2c07822
ACS Nano 2022, 16, 18936−18950

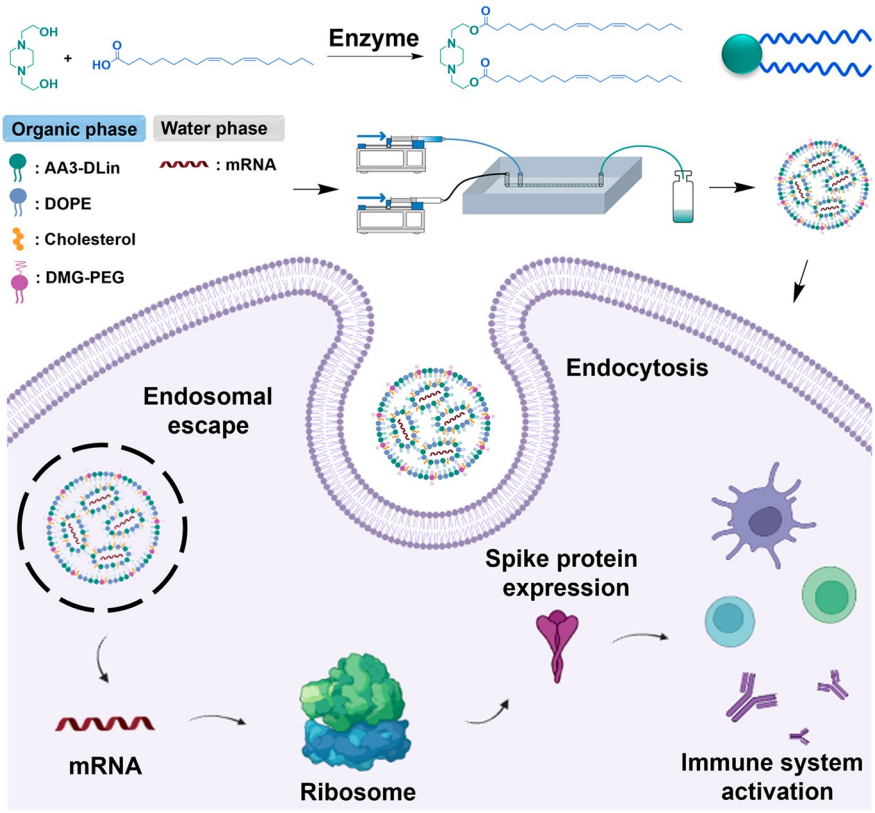

Figure 1. A schematic to illustrate the enzyme-catalyzed synthesis of ionizable cationic lipids for developing lipid nanoparticle-based mRNA COVID-19 vaccines.

mRNA therapeutics, developing high-performing ionizable cationic lipids for mRNA delivery is of great importance for next-generation gene therapeutics.[3]

The FDA-approved ionizable cationic lipids such as DLin-MC3-DMA (MC3),[7] ALC-0315,[17] and SM-102[18] are synthesized through multistep reactions and present drawbacks such as a low chemical yield especially after multiple post-reaction processes.[7,18] Moreover, most published lipid-like materials are synthesized through Michael addition or epoxide ring-opening reactions, which makes the resulting lipid-like materials non-biodegradable with potential cytotoxicity.[12,19−22] To this end, we aim to develop a strategy for high-eficiency synthesis of biodegradable ionizable cationic lipids for use in mRNA-LNP delivery platforms.

Enzyme-assisted chemical reactions have been widely employed in laboratory and industrial processes since enzymes are non-toxic, eco-friendly, recyclable biocatalysts; in particular, Candida antarctica Lipase B (CALB) is a frequently used high-eficiency biocatalyst in organic syntheses such as esterification and transesterification.[23−27] Herein, we have utilized a chemical and biological tool, the enzyme catalyst Candida antarctica Lipase B, to synthesize a chemical library of degradable ionizable cationic lipids using amino alcohols and lipid acids, resulting in 144 lipid-like materials with high chemical yield and purity. Notably, this method provides a clean and eco-friendly chemical reaction avoiding corrosive catalysts used in conventional esterification, and the enzyme can be recycled for repeated use with minimized pollution to fulfill the principles of "Green Chemistry". Through high-throughput screening, the top-performing ionizable lipid was determined to be AA3-DLin, which is rationally designed to be composed of two unsaturated linoleic lipid chains, two tertiary amine head groups from piperazine which can provide enough positive charge to condense the gene payloads in acidic buffer, and two biodegradable ester linkers.[8] To further investigate the optimized AA3-DLin LNP formulation, an orthogonal design of experiment (DoE) methodology was employed to fine-tune the molar ratios of AA3-DLin, DOPE, cholesterol, and DMG-PEG.[22,28] The optimized AA3-DLin LNP formulation shows much improved transfection eficacy over MC3 LNPs (Alnylam)[4,7] and ALC-0315 LNPs (Pfizer/BioNTech),[29] which are FDA-approved LNP formulations. Additionally, the AA3-DLin LNP formulations present an excellent capacity for long-term storage shown in the fact that mRNA-LNPs could be frozen for 12 months without transfection eficacy reduction at −20 °C. Furthermore, both fresh and 12-month frozen AA3-DLin COVID-19 vaccines elicit robust spike protein antibody titers and Th1-biased T cell responses in BALB/c mice (Figure 1). These results demonstrate the advantages of enzyme-catalyzed reactions for developing ionizable cationic lipids, and the great potential of AA3-DLin LNP delivery platforms for next-generation mRNA therapeutics.

RESULTS

Design, Synthesis, and Screening of Ionizable Cationic Lipid Library. The ideal ionizable cationic lipid is composed of three parts: (1) hydrophilic ionizable amine headgroups for condensing the mRNA, (2) hydrophobic hydrocarbon chains capable of promoting self-assembly and phospholipid membrane fusion, and (3) biodegradable linkers connecting the headgroups with hydrocarbon chains, enabling safe clearance after mRNA delivery (Figure 2A,B).[8,9,30] We

https://doi.org/10.1021/acsnano.2c07822
ACS Nano 2022, 16, 18936−18950

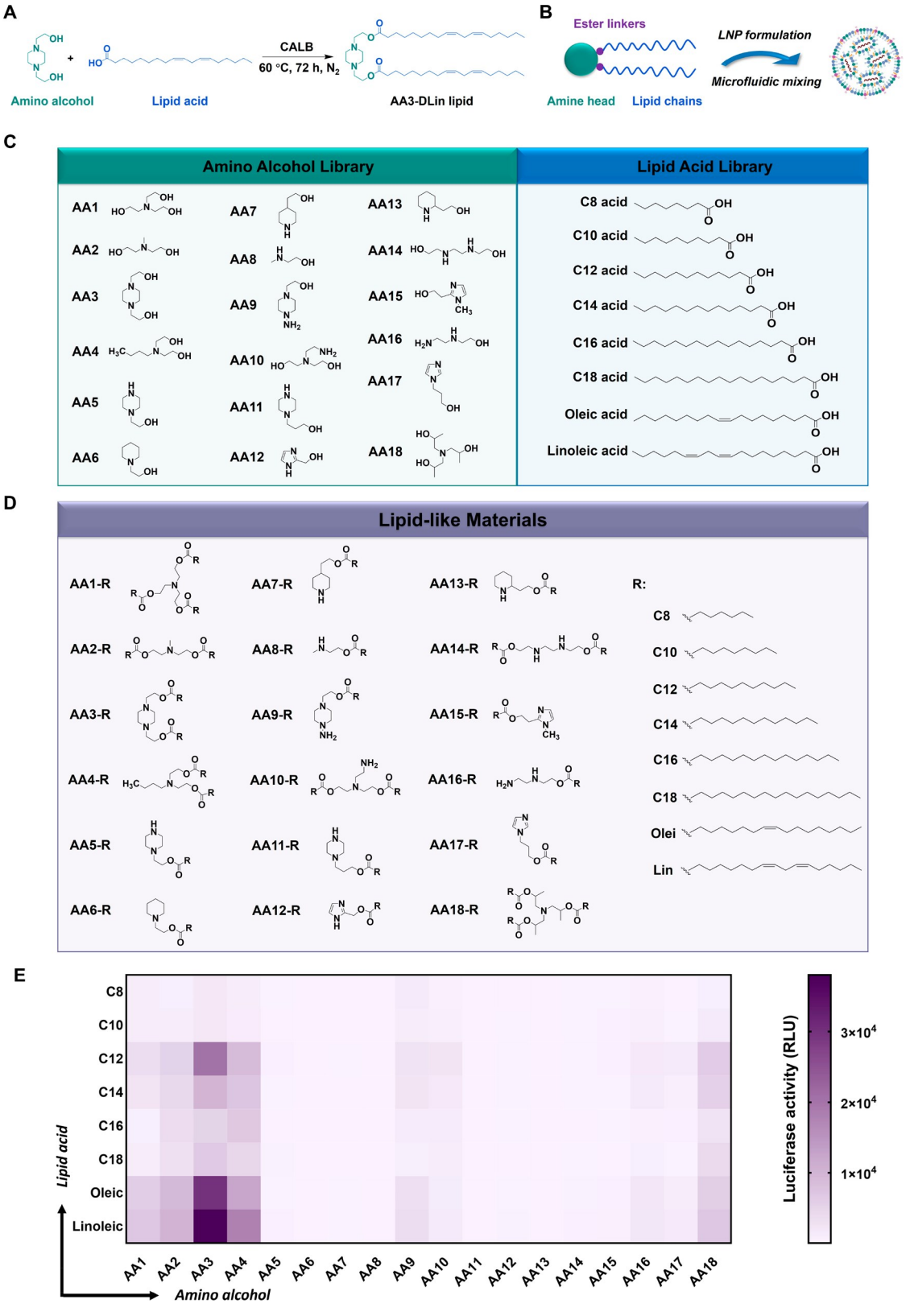

Figure 2. Synthesis and screening of the lipid-like materials. (A) The synthesis of AA3-DLin through enzyme-catalyzed esterification. (B) A schematic to illustrate the rational design of ionizable cationic lipid. (C) Chemical structure of amino alcohols and lipid acids used in the synthesis of lipid-like materials. (D) The chemical structures of 18*8 lipid-like materials where "R" represents different saturated or unsaturated alkyl chains. (E) Luciferase expression heat map of mLuc-loaded LNPs. The LNPs were prepared with different lipid-like materials. *X*-axis represents different amino alcohols. *Y*-axis displays different lipid acids used for synthesis. All the LNPs were prepared with synthesized lipids, DOPE, cholesterol, and DMG-PEG with a molar ratio of 50:10:38.5:1.5 and a 1:20 weight ratio of mRNA to lipid (wt./wt.). All the transfection experiments were repeated in triplicate, and the expression heat map was generated by mean values.

https://doi.org/10.1021/acsnano.2c07822
ACS Nano 2022, 16, 18936−18950

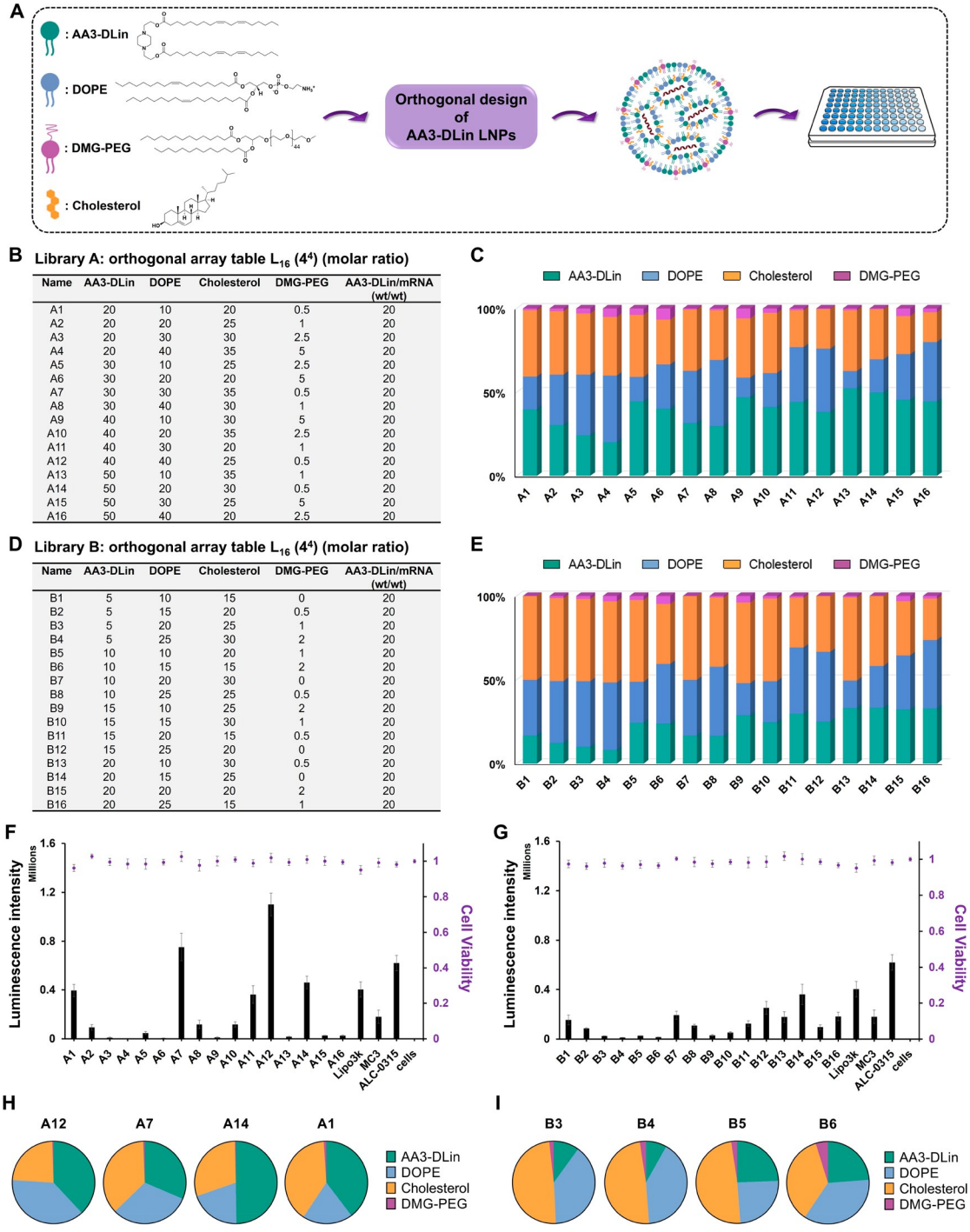

Library A: orthogonal array table L_{16} (4^4) (molar ratio)

Name	AA3-DLin	DOPE	Cholesterol	DMG-PEG	AA3-DLin/mRNA (wt/wt)
A1	20	10	20	0.5	20
A2	20	20	25	1	20
A3	20	30	30	2.5	20
A4	20	40	35	5	20
A5	30	10	25	2.5	20
A6	30	20	20	5	20
A7	30	30	35	0.5	20
A8	30	40	30	1	20
A9	40	10	30	5	20
A10	40	20	35	2.5	20
A11	40	30	20	1	20
A12	40	40	25	0.5	20
A13	50	10	35	1	20
A14	50	20	30	0.5	20
A15	50	30	25	5	20
A16	50	40	20	2.5	20

Library B: orthogonal array table L_{16} (4^4) (molar ratio)

Name	AA3-DLin	DOPE	Cholesterol	DMG-PEG	AA3-DLin/mRNA (wt/wt)
B1	5	10	15	0	20
B2	5	15	20	0.5	20
B3	5	20	25	1	20
B4	5	25	30	2	20
B5	10	10	20	1	20
B6	10	15	15	2	20
B7	10	20	30	0	20
B8	10	25	25	0.5	20
B9	15	10	25	2	20
B10	15	15	30	1	20
B11	15	20	15	0.5	20
B12	15	25	20	0	20
B13	20	10	30	0.5	20
B14	20	15	25	0	20
B15	20	20	20	2	20
B16	20	25	15	1	20

Figure 3. Orthogonal design of experiment methodology for screening the optimized formulation of AA3-DLin LNPs. (A) A schematic illustrates the four components of AA3-DLin LNPs for Design of Experiment (DoE) calculation. Two L_{16} (4^4) orthogonal tables were employed to guide the optimization of LNP formulations. (B) Details of LNP formulations in Library A for first-round optimization, including the determinate molar ratios of each component in AA3-DLin LNPs. (C) Molar ratios of the orthogonally designed AA3-DLin LNPs in Library A. (D) Details of LNP formulations in Library B for second-round optimization. (E) Molar ratios of the orthogonally designed AA3-DLin LNPs in Library B. (F) The transfection eficacy and cell viability of different AA3-DLin LNP formulations in Library A with MC3 LNPs, ALC-0315 LNPs and lipofectamine 3000 were evaluated on Hek 293 cells. (G) The transfection eficacy and cell viability of LNP formulations in Library B were evaluated on Hek 293 cells. (H) The composition of the top-performing AA3-DLin LNP formulations. (I) The composition of the worst-performing AA3-DLin LNP formulations. Cell viability data were normalized to control groups. Experiments were carried out in triplicate to get results. Data are displayed as mean ± SD.

rationally designed a chemical structure library of ionizable cationic lipids where the ionizable amine headgroups originated from amino alcohols and the hydrocarbon chains were derived from lipid acids (Figure 2C). Through CALB enzyme-assisted reaction, the hydroxyl groups were reacted with carboxylic acids via a one-step high-eficiency esterification, and a library of 18*8 lipid-like materials was synthesized by varying amino alcohols and lipid acids (Figure 2D).[24] The

https://doi.org/10.1021/acsnano.2c07822
ACS Nano 2022, 16, 18936−18950

A

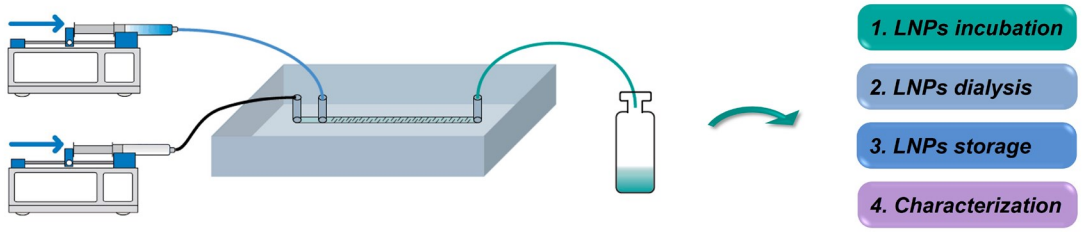

B

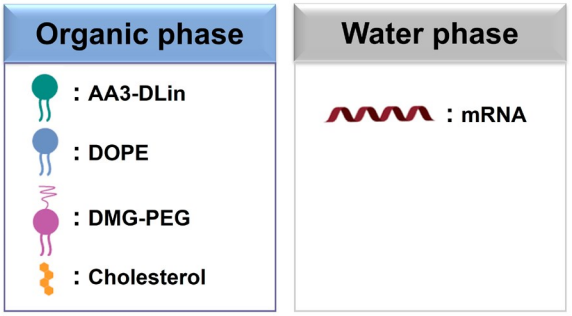

C

AA3-DLin LNP formulation (molar ratio)			
AA3-DLin	DOPE	Cholesterol	DMG-PEG
40	40	25	0.5
AA3-DLin LNP formulation (molar percentage)			
AA3-DLin	DOPE	Cholesterol	DMG-PEG
38.0%	38.0%	23.7%	0.3%

D

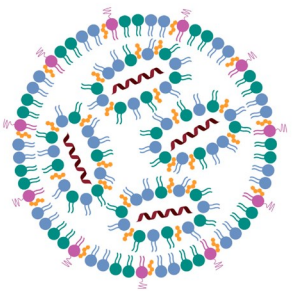

E

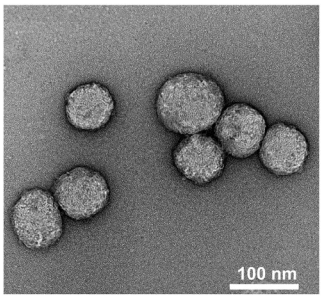

F

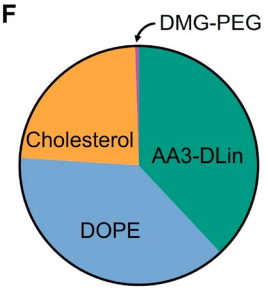

G

Water phase (μL/min)	Organic phase (μL/min)	W/O ratio	Size (nm)	PDI	Zeta potential (mV)	Encapsulation efficacy (%)
300	100	3:1	156.5 ± 11.8	0.168 ± 0.032	-3.2 ± 2.1	91.8 ± 3.6
900	300	3:1	114.6 ± 5.3	0.156 ± 0.025	-4.6 ± 3.5	93.2 ± 1.5
1500	500	3:1	96.2 ± 4.1	0.132 ± 0.016	-4.2 ± 2.2	95.7 ± 0.8
2400	800	3:1	89.7 ± 3.8	0.128 ± 0.012	-2.8 ± 2.6	96.5 ± 1.2

H

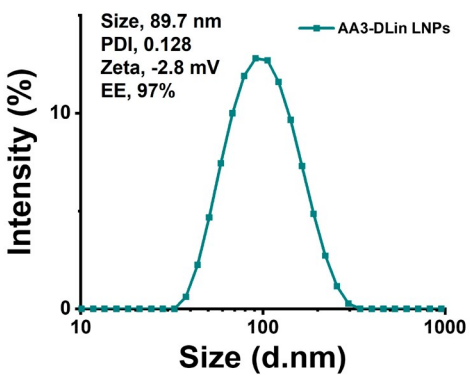

I

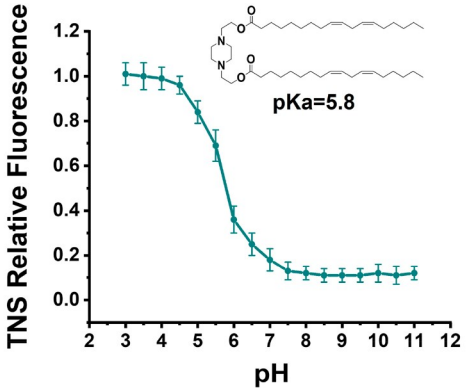

Figure 4. Fabrication and characterization of AA3-DLin LNPs prepared by microfluidic device. (A) A general schematic illustration of AA3-DLin LNP fabrication through microfluidic mixing with the following preparation processes. (B) Formulation of AA3-DLin LNPs where the organic phase contains AA3-DLin, DOPE, cholesterol, and DMG-PEG, the water phase contains the mRNA of interest in NaOAc buffer (25 mM, pH 5). (C) The determinate AA3-DLin LNP formulation after orthogonal DoE screening. (D) A schematic illustration of the AA3-DLin LNP structure: the outer layer is composed of four components listed and the mRNAs were encapsulated inside LNPs via electrostatic interactions. (E) TEM image of AA3-DLin LNPs stained by uranyl acetate solution (scale bar: 100 nm). (F) The molar percentage of the

https://doi.org/10.1021/acsnano.2c07822
ACS Nano 2022, 16, 18936−18950

Figure 4. continued

optimized AA3-DLin LNP formulation. (G) Characterizations of AA3-DLin LNPs fabricated by a microfluidic device with different syringe pump rates. The LNP size can be controlled by varying the pump rates. (H) Characterization summary of the optimized LNPs prepared through microfluidic device under high pump rate, with a molar ratio of 40:40:25:0.5 (AA3-DLin/DOPE/cholesterol/DMG-PEG). (I) The pK_a value of AA3-DLin LNPs, defined as the pH at half-maximal fluorescence intensity. Experiments were carried out for three times to get results. Data are presented as mean ± SD.

mechanism of CALB-catalyzed esterification is described in Figure S1.[31,32] Notably, the one-step CALB enzyme-catalyzed esterification led to a high-throughput and eco-friendly synthesis of the lipid-like material library with high chemical yield and product purity (Table S1). We preliminarily fabricated these lipid-like materials to form LNPs at a molar ratio of 50:10:38.5:1.5 (ionizable lipid: DOPE: cholesterol: DMG-PEG). We chose this molar ratio initially because it is the most widely used to deliver mRNA.[7,8] We then proceeded to deliver luciferase encoded mRNA (mLuc) *in vitro* and generated a luciferase expression heat map using the formulated LNPs (Figure 2E). The top-performing lipid was screened and termed AA3-DLin which was chemically composed of 1,4-Bis(2-hydroxyethyl) piperazine amine headgroups connected with two linoleic lipids by ester linkers (Figure 2A). The AA3-DLin lipids were successfully synthesized by high-eficiency CALB-catalyzed esterification with 85% chemical yield and 96% purity without detectable byproduct and further characterized by electrospray ionization (ESI) mass spectrometry, which showed a strong, clear, and single peak denoting AA3-DLin with molecular weight (MW) of 699 (Figure S2). Furthermore, nuclear magnetic resonance (NMR) spectroscopy and Fourier-transform infrared spectroscopy (FTIR) revealed the chemical structure of AA3-DLin accordingly in Figure S3 and S4. Additionally, the AA3-DLin lipids were further synthesized by traditional esterification catalysts, concentrated H_2SO_4 and DMAP. The chemical yield of concentrated H_2SO_4 catalyzed AA3-DLin and DMAP catalyzed AA3-DLin are ⍰45% and ⍰72%, respectively (Table S1).[18,33] These results showed the superiority of CALB enzyme in catalyzing the synthesis of AA3-DLin lipids.

Screening of AA3-DLin LNP Formulation by Orthogonal Design of Experiment Methodology. The mRNA delivery eficacy is not solely determined by the ionizable cationic lipid; the ratio of these four ingredients in the LNPs can also exert a significant effect. Therefore, to optimize the AA3-DLin LNP formulation, an orthogonal design of experiment (DoE) methodology was carried out to fine-tune the molar ratios of AA3-DLin, DOPE, cholesterol, and DMG-PEG (Figure 3A).[22,28,34,35] The orthogonal design was used to screen 256 (4^4) possible LNP formulations by combining four excipients of AA3-DLin, DOPE, cholesterol, and DMG-PEG with 16 formulations and evaluate four components with only 16 typical combinations. For the first-round optimization (Library A), the relative molar ratios and molar percentages of the four components in LNP formulation are described in Figure 3B,C, respectively. Briefly, formulations were prepared with the following ratios of AA3-DLin (20 to 50): DOPE (10 to 40): cholesterol (20 to 35): DMG-PEG (0.5−5), and a fixed 1:20 (wt./wt.) weight ratio of mRNA to AA3-DLin. To further screen the formulation, a second round of optimization (Library B) was conducted where the relative molar ratios and molar percentages were fine-tuned as described in Figure 3D,E. The physiochemical characterizations and detailed formulations of the orthogonally designed LNPs are described in Table S2−S7. The mLuc was used as a quantitative reporter signal to evaluate the transfection eficacy of LNPs on Hek 293 cells with the FDA-approved MC3 LNPs,[7] ALC-0315 LNPs,[29] and commercial lipofectamine 3000 as control groups.

From the analysis of Figure 3F,G, we found that increasing the proportion of DMG-PEG dramatically lowers the transfection eficacy of AA3-DLin LNP *in vitro*. However, the DMG-PEG is also very important for LNP transfection *in vivo* as it prevents immune system detection of LNPs.[5] Therefore, to enhance AA3-DLin LNP transfection eficacy, DMG-PEG was optimized to 0.5 (molar ratio) in the AA3-DLin LNP formulation. Notably, all the top-performing formulations have relatively high proportions of AA3-DLin and DOPE such as A12, A7, A14, and A1 (Figure 3H), and all the worst-performing formulations have low proportions of AA3-DLin such as B3, B4, B5, and B6 (Figure 3I). Different from the FDA-approved siRNA-LNP formulations that frequently require high proportions of ionizable cationic lipids and low proportions of phospholipids,[7,8] we found that a high proportion of both ionizable cationic lipids (AA3-DLin) and phospholipids (DOPE) dramatically enhances the mRNA transfection eficacy *in vitro*. We hypothesize that a high proportion of fusogenic DOPE facilitates LNP fusion into cells by adopting an inverted hexagonal H(II) phase which facilitates endosomal release of encapsulated mRNA by destabilizing endosomal membranes to enhance the protein translation.[4,5,10,34] Consequently, through high-throughput screening, the A12 formulation with a molar ratio of 40:40:25:0.5 (AA3-DLin/DOPE/cholesterol/DMG-PEG) was determined to be the optimized formulation of AA3-DLin LNPs which showed a 6-fold, 3-fold and 2-fold higher transfection eficacy than MC3 LNPs, lipofectamine 3000 and ALC-0315 LNPs *in vitro*, respectively (Figure 3F). Moreover, degradability is an essential characteristic of lipids which improves biosafety and lowers cytotoxicity. The data showed that AA3-DLin is a degradable material in aqueous PBS (pH 7.4) solution via hydrolysis of ester bonds (Figure S5). No cytotoxicity was observed for any of the AA3-DLin LNP formulations after 1 day post-transfection at 1:20 weight ratio of mRNA to AA3-DLin (wt./wt.), which demonstrated the excellent biosafety of AA3-DLin LNPs (Figure 3F,G).

Microfluidic Fabrication and Characterization of LNPs. Besides the ionizable cationic lipid and the LNP formulation ratios, the nanoparticle size also affects the transfection eficacy and vaccine immunogenicity.[36] Microfluidic-chip device is a LNP fabrication method used to obtain uniform nanoparticles (Figure 4A).[37] AA3-DLin, DOPE, cholesterol, and PEGylated lipid were dissolved separately in ethanol at 10 mg/mL and mixed at a molar ratio of 40:40:25:0.5 to obtain the organic phase (Figure 4B,C,F). Additionally, the mRNA water phase was prepared by dissolving the mRNA of interest in sodium acetate (NaOAc) buffer. The volume ratio of lipid organic phase to mRNA aqueous phase was fixed at 1:3 (v./v.) and separately loaded into different syringes. The LNP production process is detailed

https://doi.org/10.1021/acsnano.2c07822
ACS Nano 2022, 16, 18936−18950

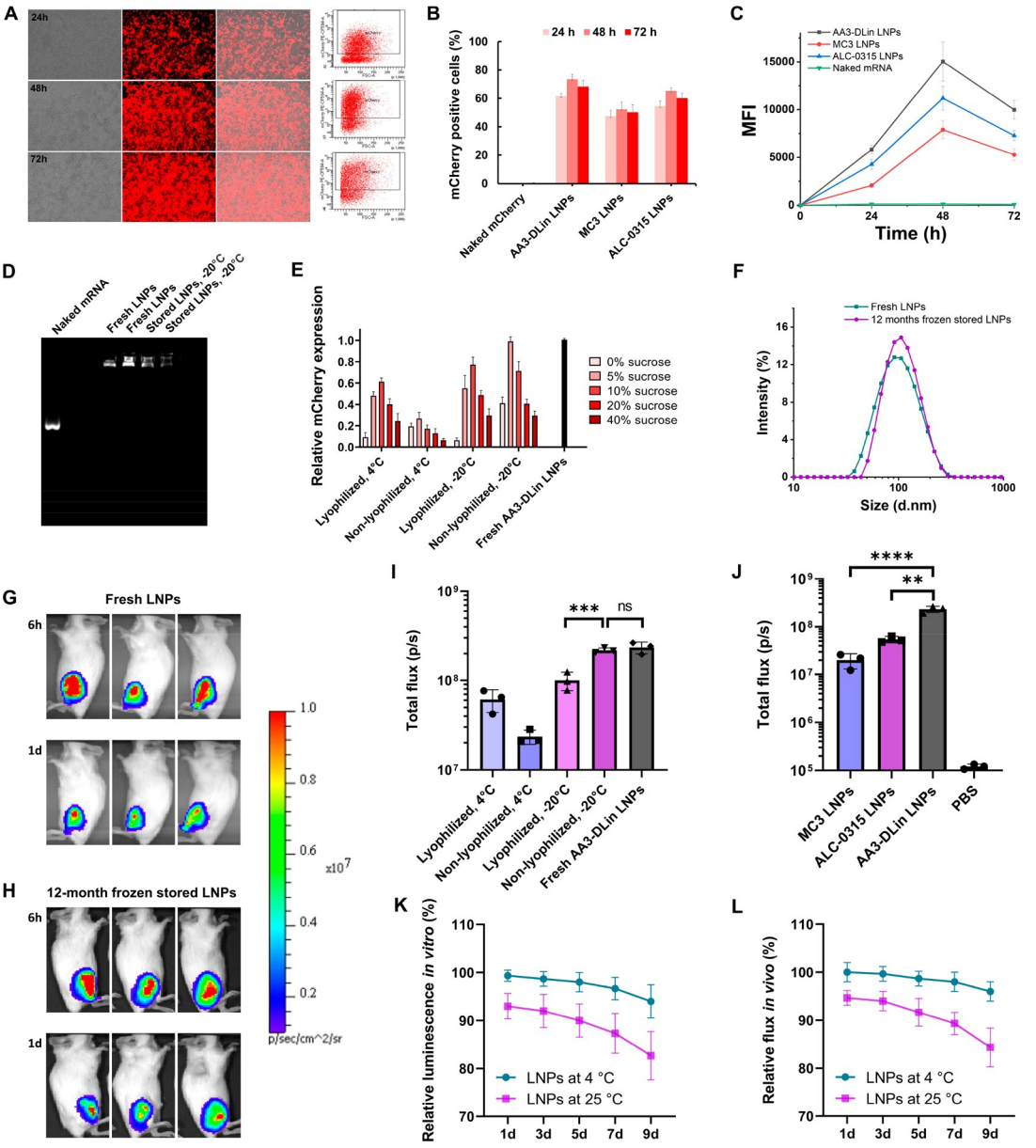

Figure 5. Comprehensive evaluation of AA3-DLin LNPs. (A) The fluorescence images and flow cytometry results of mCherry-positive Hek 293 cells transfected by AA3-DLin LNPs. (B) Summary of mCherry-expressing cell population transfected by different LNP formulations. (C) MFI of mCherry-expressing cells based on the flow cytometry results. (D) The mRNA binding analysis was characterized by agarose gel electrophoresis for both fresh and 12-month frozen stored AA3-DLin mRNA-LNPs. (E) Transfection evaluation of 12-month stored mCherry-LNPs *in vitro*, the data were summarized by flow cytometry and normalized to fresh LNPs. (F) The comparison of AA3-DLin LNP size and distribution between fresh and 12-month frozen stored LNP formulations. (G) Bioluminescence images of fresh mLuc-LNPs ($n = 3$) treated BALB/c mice and (H) 12-month frozen mLuc-LNPs. (I) Summary of luciferase expression generated by different 12-month stored mLuc-LNP formulations *in vivo*, the luciferase expression was recorded after 6 h post-injection. (J) Comparison of the transfection eficacy of different FDA-approved LNP formulations. The luciferase expression was recorded after 6 h post-injection. (K) The thermostability evaluation of AA3-DLin LNPs *in vitro*. The luciferase expression was recorded after 1 day post-transfection on Hek 293 cell line and the luminescence intensity was normalized to fresh mLuc-LNPs. (L) The thermostability evaluation of AA3-DLin LNPs *in vivo*. The luciferase expression was recorded after 6 h post-injection on BALB/c mice and the total flux was normalized to fresh mLuc-LNPs. Experiments were performed in triplicate. Data were displayed as means ± SD. The unpaired *t* test was carried out to analyze the significance difference between two groups (ns, not significant; *$p < 0.05$, **$p < 0.01$, ***$p < 0.001$, ****$p < 0.0001$).

in the following steps: (1) the two material phases were pumped and rapidly mixed in the microfluidic channels to obtain uniform LNPs; (2) the resulting LNPs were incubated at room temperature (RT) for 20 min allowing for mRNA encapsulation; (3) the LNPs were further dialyzed against 1×PBS for 2 h at RT to remove the ethanol. Then the LNPs were ready for characterization, storage, and administration in animal studies (Figure 4A). In the microfluidic device, the two phases were rapidly pumped and thoroughly mixed to obtain uniform LNPs through the micro-sized channels where the positively charged headgroup of the AA3-DLin lipid can electrostatically interact with negatively charged mRNAs in an acidic buffer and allow mRNA encapsulation inside LNPs (Figure 4D). The TEM image clearly shows that the AA3-

https://doi.org/10.1021/acsnano.2c07822
ACS Nano 2022, 16, 18936−18950

DLin LNPs have a diameter around 90 nm in particle size which is consistent with the DLS result (Figure 4E,H). Additionally, the nanoparticles displayed a uniform compact spherical shape, and no differences were observed in the morphology of the AA3-DLin LNPs compared to other published LNPs.[38−41]

Notably, we observed that the LNP size can be adjusted by controlling the pump rates. By increasing pump rate to 2400 μL/min for the water phase and 800 μL/min for the organic phase, the LNPs obtained were 89 nm in size with a 0.128 polydispersity index (PDI). At low pump rates, the resulting size of LNPs ranged from 114.6 to 156.5 nm. Additionally, adjusting the pump rates did not distinctly affect the zeta potential and encapsulation eficacy of the LNPs exemplified by the fact that all the obtained LNPs have a neutral zeta potential and more than 90% encapsulation eficacy (Figure 4G). Moreover, the pK_a is an important characteristic of the ionizable cationic lipid which signifies the pH when LNPs are 50% protonated. This indicates the region where LNPs become cationic and interact with the endosomal membrane leading to the release of the mRNA to cytoplasm for protein translation.[7,11,42] The pK_a of AA3-DLin LNPs was evaluated by analyzing the fluorescence intensity of 2-(*p*-toluidino)-6-napthalene sulfonic acid (TNS). The formulated AA3-DLin LNPs were titrated from pH 3.0 to 11.0, and an "S" curve was generated. After a curve-fit analysis, the pK_a of AA3-DLin LNPs was determined to be 5.8, which was the pH value at 50% of maximum fluorescence (Figure 4I). Additionally, the pK_a values of top lipid candidates in the material library were all in the range of 4 to 7 (Figure S6), which shows the potential for lipids to be protonated in acidic environment for mRNA delivery and the advantageous design of the synthesized lipid-like material library.[4]

Comprehensive Evaluations of AA3-DLin LNPs *in Vitro* and *in Vivo*. Evaluations of AA3-DLin LNP transfection eficacy were performed *in vitro* and *in vivo*, where the optimized AA3-DLin LNP formulations were prepared by a microfluidic device with the mRNA of interest. First, the *in vitro* transfection eficacy of AA3-DLin LNPs were evaluated by delivering mCherry encoded mRNA (mCherry-LNPs) to Hek 293 cells. The images of mCherry-positive cells were captured by a fluorescence microscope and further analyzed by flow cytometry (Figure 5A). The flow cytometry results showed the percentage of mCherry transfected cells reached around 78% at 48 h post-transfection, whereas the FDA-approved MC3 LNPs and ALC-0315 LNPs groups showed the population of mCherry-expressing cells at 58% and 65% (Figure 5B). Additionally, the mean fluorescence intensity (MFI) comparison study of mCherry-expressing cells showed that the AA3-DLin LNPs outperformed the other LNP groups (Figure 5C). Next, the mLuc was delivered by the AA3-DLin LNPs to investigate the transfection eficacy *in vivo*. The mLuc-LNPs were intramuscularly injected into BALB/c mice. Notably, the AA3-DLin LNPs eficiently delivered the mLuc *in vivo* and generated strong luciferase expression at 2.35×10^8 total flux (p/s) at 6 h post-injection (Figure 5G). The comparison studies were performed with FDA-approved MC3 LNPs[7] and ALC-0315 LNPs[29] through intramuscular injection of mLuc under same preparation conditions. The total flux was recorded at 6 h post-injection, and the results demonstrated that the AA3-DLin LNP formulations outperformed these commercial FDA-approved LNP formulations (Figure 5J).

We then explored the long-term storage capability of AA3-DLin LNPs under different storage conditions. Sucrose was formulated into AA3-DLin LNP as the cryoprotectant to stabilize LNP structure during storage.[43,44] Previous reports showed that sucrose was the most effective cryoprotectant with high viscosity and low molecular mobility, and serves as a stabilizer to minimize the van der Waals interaction and preserve the spacing between the nanoparticles during frozen storage.[23,43,45] A sucrose solution was added to LNPs with final concentrations of 0−40 wt % and the resulting LNPs were further lyophilized as dry powder or stored at 4 °C and −20 °C with a timeline of 12 months. The transfection eficacy of stored LNPs was characterized *in vitro* and *in vivo* with the fresh LNPs as the positive control. After 12 months at −20 °C, the frozen (nonlyophilized) mCherry-LNPs with 5 wt % sucrose showed no reduction in transfection eficacy compared with the fresh LNPs (Figure S7). However, after 12 months storage at 4 °C, mCherry-LNPs solution (nonlyophilized) exhibited a dramatic decrease in transfection eficacy, probably due to the hydrolysis-mediated degradation of LNPs and mRNAs. For the lyophilized mCherry-LNPs, the best sucrose concentration was determined to be 10 wt % after analysis and the lyophilized LNPs showed a moderate decrease in transfection eficacy compared to fresh LNP after 12-month storage at −20 °C (Figure 5E). Furthermore, we characterized the 12-month stored mLuc-LNPs in BALB/c mice where the frozen LNPs and lyophilized LNPs were fixed with 5 and 10 wt % sucrose, respectively. Notably, the frozen mLuc-LNPs showed no reduction in transfection eficacy compared with fresh LNPs after 12-month frozen storage at −20 °C (Figure 5H,I) and still generated strong luciferase expression ≈ 2.21×10^8 total flux (p/s) at 6 h postadministration. However, the lyophilized LNPs showed a loss of transfection eficacy, from 2.35×10^8 to 1.02×10^8 total flux (p/s) *in vivo* over 12 months (Figure 5I). We hypothesize that the oxidization of unsaturated lipids in the lyophilized LNPs leads to the loss of transfection eficacy during storage since the degree of unsaturation of lipids has a positive effect on LNP transfection eficacy.[46]

The agarose gel electrophoresis results demonstrated that the fresh and 12-month frozen AA3-DLin LNPs bound mRNAs eficiently at 1:10 weight ratio of mRNA/AA3-DLin (Figure 5D). Moreover, the 12-month frozen stored mLuc-LNPs represented excellent stability where the particle size slightly changed from 89 to 105 nm with no obvious change in PDI and zeta potential compared to fresh LNPs (Figure 5F). The nanoparticle stability results showed the AA3-DLin LNPs maintained mRNA delivery eficacy *in vitro* and *in vivo* at 4 °C for 1 week (Figure 5K,L). Furthermore, the muscular tissue immunofluorescence assay for proinflammatory biomarker IL-6 and histopathology were evaluated after administration of AA3-DLin LNP 5 days postinjection. Tissue images indicated that there was no AA3-DLin LNP induced inflammation detected after comparison with PBS control groups (Figure S8 and S9).[47−49]

Evaluation of AA3-DLin mRNA COVID-19 Vaccine *in Vitro*. AA3-DLin mRNA vaccines were developed by encapsulating full-length spike protein (Figure S10) encoded mRNA.[2,50,51] The AA3-DLin vaccines were formulated with 5 wt % sucrose and frozen for 12 months at −20 °C before vaccination studies. The AA3-DLin vaccines delivered spike mRNA eficiently in the Hek 293 cells with strong spike protein expression demonstrated by Western Blot and

https://doi.org/10.1021/acsnano.2c07822
ACS Nano 2022, 16, 18936−18950

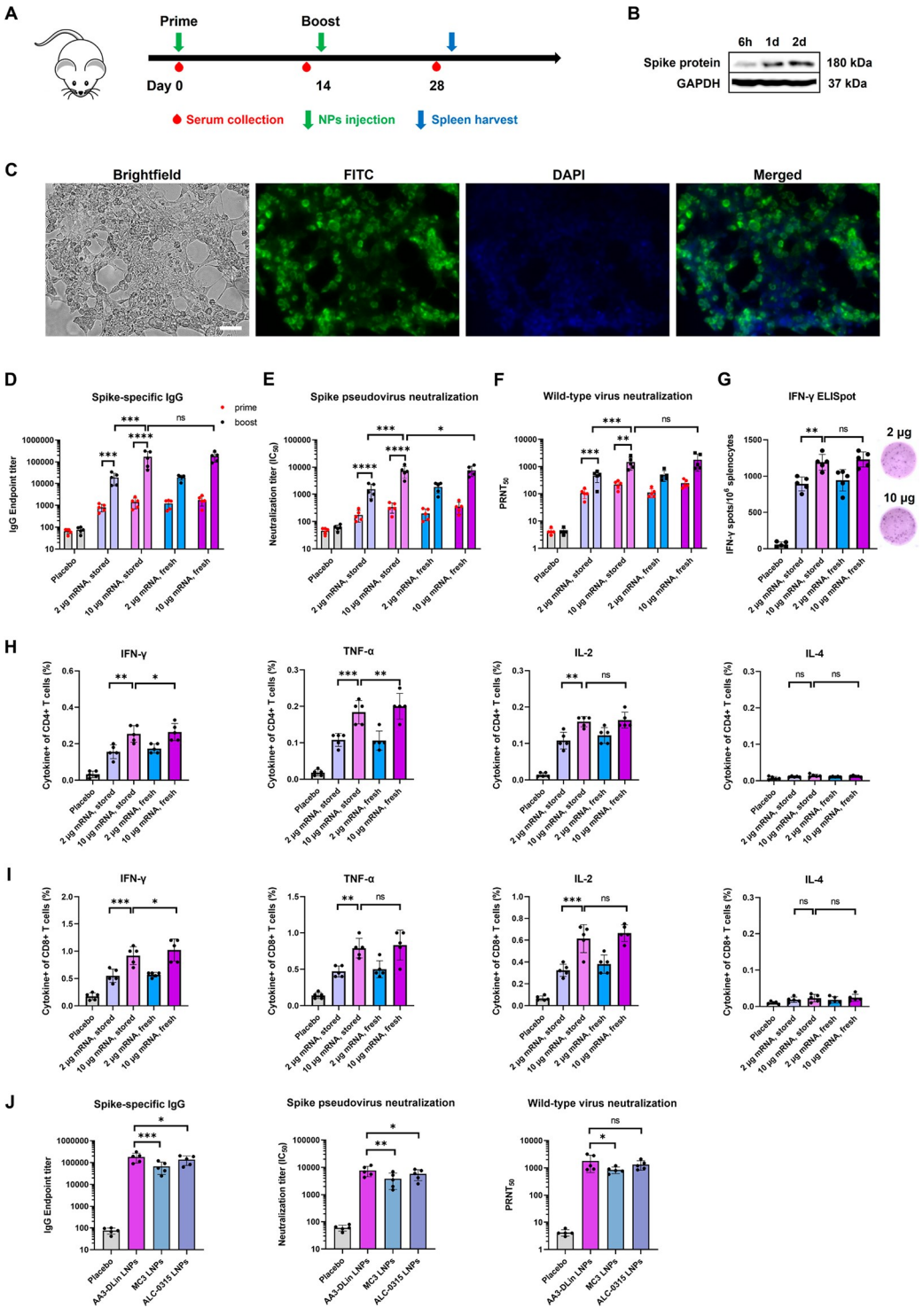

Figure 6. Immunogenicity of AA3-DLin COVID-19 vaccines. (A) Schematic illustration of mice immunization experimental design. (B) Western Blot analysis of spike protein expression by AA3-DLin vaccines. (C) Immunofluorescent staining of spike protein after transfection by AA3-DLin vaccines (scale bar, 50 μm). (D) AA3-DLin vaccines induced robust SARS-CoV-2 spike-specific antibody endpoint titers in the immunized mice. (E) IC_{50} titers of spike pseudovirus neutralizing antibody. (F) $PRNT_{50}$ titers of AA3-DLin vaccines in the immunized mouse sera. (G) IFN-γ secretion was evaluated using ELISpot assay of the stimulated splenocytes along with representative images of ELISpot plate wells. (H) The populations IFN-γ, TNF-α, IL-2, and IL-4 positive CD4+ and (I) CD8+ T cells in vaccinated mice groups. (J) Comparison studies of spike-specific antibody generated by different LNP formulations. Spike-specific IgG endpoint titers (left), spike pseudovirus neutralizing antibody IC50 titers (middle) and ($PRNT_{50}$) titers (right) were evaluated using AA3-DLin LNPs, MC3 LNPs, and ALC-0315 LNPs, n = 5. All LNPs were encapsulated with 10 μg spike-encoded mRNA, and serum was collected after second booster injection at day 28. Data are displayed as means ± SD. A one-way ANOVA with multiple comparison tests and unpaired t test for comparison of two groups were used to analyze the statistical significance (ns, not significant; *$p < 0.05$, **$p < 0.01$, ***$p < 0.001$, ****$p <$ 0.0001).

https://doi.org/10.1021/acsnano.2c07822
ACS Nano 2022, 16, 18936−18950

immunofluorescence analysis. The AA3-DLin vaccine transfected lysates exhibited clear full-length spike protein bands at ⍰180 kDa with GAPDH as the loading control (Figure 6B). Additionally, the expressed spike protein was also probed by fluorescence-labeled antibodies (Figure 6C).

Immunogenicity Evaluation of AA3-DLin COVID-19 Vaccine *in Vivo*. Groups of BALB/c mice (n = 5) were intramuscularly injected with different mRNA dosages (2 μg and 10 μg) of 12-month frozen stored and fresh AA3-DLin vaccines with the empty LNP group as the placebo group. A prime/boost manner of vaccination was applied to each group 2 weeks apart. The serum samples were collected at preset time points and the spleens were harvested at the end of immunization studies (Figure 6A). Moderate SARS-CoV-2 spike-specific antibodies were recognized by enzyme-linked immunosorbent assay (ELISA) post-prime injection of both fresh and long-term stored AA3-DLin vaccines after 13 days. The AA3-DLin vaccines induced geometric mean titers (GMTs) of antibodies ranging from 808 to 1550. Additionally, the spike pseudovirus neutralization study demonstrated that GMTs of neutralizing antibody 50% inhibitory concentration (IC50) ranged from 176 to 340. On day 14, the booster doses were administered, and the serum samples were collected at day 28. The antibody levels increased significantly with a dose-dependent relationship exemplified by the GMTs of antibodies rising to 19 118 (2 μg) and 181 875 (10 μg) (Figure 6D). Additionally, the pseudovirus IC50 GMTs also showed a dose-dependent increase and reached 1520 (2 μg) to 7740 (10 μg) (Figure 6E). Moreover, a 50% plaque reduction neutralization test ($PRNT_{50}$) was performed for the real virus challenge studies, and the results are shown in Figure 6F. It is worthwhile to note that no obvious spike-specific antibodies were detected in the empty LNP placebo group. Overall, the GMTs of spike-specific antibody were actively related with pseudovirus neutralizing IC50 GMTs as well as $PRNT_{50}$ antibody titers, and AA3-DLin vaccines elicit strong spike-specific antibody responses in the immunized mice after booster injections.

Furthermore, intracellular cytokine staining was performed to evaluate the T cell immune responses in the immunized mice. The splenocytes were isolated from vaccinated and placebo groups of mice following stimulation with peptide pools which covered the SARS-CoV-2 spike glycoprotein immunodominant sequence domains. Intracellular cytokine staining (ICS) and enzyme-linked immunosorbent spot (ELISpot) were utilized to measure spike-specific T cell responses. The cell populations of interferon gamma (IFN-γ), interleukin-2 (IL-2), tumor necrosis factor alpha (TNF-α), and interleukin-4 (IL-4) expressing CD4+ and CD8+ T cells were characterized by flow cytometric analysis with the indicated gating strategy (Figure S11). The results showed both fresh and stored AA3-DLin vaccinated mice present a significantly higher cell population of IFN-γ+, IL-2+, and TNF-α+ cytokine-expressing T cells than the placebo group with a dose−response relationship (Figure 6H,I). Furthermore, there is no detectable secretion of IL-4 cytokine in either placebo-vaccinated mice or AA3-DLin vaccine immunized groups. This demonstrates that AA3-DLin vaccines successfully elicit Th1-biased T cell responses in the immunized mice. Additionally, an IFN-γ ELISpot study was further performed, and the IFN-γ spots were counted as 892 (2 μg) and 1190 (10 μg) per 10^6 splenocytes, which is much higher compared to the placebo groups as shown in Figure 6G. Moreover, comparison studies of spike-specific antibodies generated by different LNP formulations were performed, and the results are shown in Figure 6J, which showed that the AA3-DLin LNPs outperformed MC3 and ALC-0315 LNPs in terms of antibody titers in the vaccinated mice sera.

DISCUSSION

The COVID-19 pandemic led to the expedited development of mRNA-LNP delivery platforms for vaccines, gene therapies, and cell therapies, especially for infectious diseases and cancer.[6] Ionizable cationic lipids which alter charge density in different pH environments have been developed to eficiently deliver gene payloads and solve safety issues of conventional cationic lipids which trigger toxic pro-apoptotic and pro-inflammatory effects.[7,52] Therefore, ionizable cationic lipids are the most essential component of mRNA-LNP delivery platforms, determining the mRNA transfection eficacy and therapeutic effect. The developed ionizable cationic lipid AA3-DLin is synthesized through an exquisite one-step biological enzyme-assisted high-eficiency esterification to avoid multiple-step chemical reactions, which are limited by a low product yield and complicated synthesis/purification processes. Unlike traditional chemical-catalyzed methods which suffer from corrosive, hazardous chemicals, and pollution, CALB-catalyzed processes have many advantages such as mild temperature reaction conditions, easier product separation, recyclable enzymes with less pollution, and high catalytic activity.[24−27,53,54] These characteristics provide a high-eficiency, eco-friendly CALB-assisted reaction which lends itself to environmentally safe scale-up by avoiding corrosive catalysts and pollution, which fulfills “Green Chemistry” principles. We believe this CALB enzyme-catalyzed synthesis method is of great potential to be generalized for synthesis of ester-bond-containing biodegradable lipids or lipid-like intermediates for gene delivery.

The orthogonal design of experiment methodology was utilized to screen the most optimized AA3-DLin LNP formulations, which have both high proportions of AA3-DLin and DOPE, to maximize mRNA delivery potential. Moreover, the microfluidic mixing device enables size-controlled fabrication of AA3-DLin LNPs by adjusting pump rates to obtain around a 100 nm particle size, which has been previously reported to induce optimal immunogenicity in mRNA-LNP vaccine systems.[36] In terms of stability evaluation, AA3-DLin LNPs exhibit improved thermostability at 4 °C for 7 days over the AA3-DLin lipid, which shows a quick hydrolysis-mediated degradation at 4 °C. We hypothesize that when the LNPs are formed, the AA3-DLin condenses with mRNA to become compact nanoparticle structures via electrostatic interaction, which prevents the hydrolysis of LNPs due to the resulting nanoparticles providing limited boundary surface for aqueous solution contact with the AA3-DLin. Moreover, there is no detectable degradation of AA3-DLin at −20 °C for at least 14 days and this fact also supports the long-term storage capability of AA3-DLin LNPs at −20 °C. The AA3-DLin LNPs are capable of being frozen for 12 months at −20 °C without reduction of mRNA delivery eficacy, which provides mRNA-LNP COVID-19 vaccines with a feasible storage methodology to potentially solve the issues of ultracold transportation and long-term storage.

This study, although comprehensive, has some limitations. First, a comparison study of immunogenicity as induced by commercial mRNA-LNP vaccines was not performed. Commercial vaccines utilize optimized gene sequences and

https://doi.org/10.1021/acsnano.2c07822
ACS Nano 2022, 16, 18936−18950

pseudouridine nucleosides in spike encoded mRNA synthesis, which shows improved immunogenicity over the wild-type spike mRNA.[55−57] This work is mainly focused on using enzyme-catalyzed chemical-biological synthesis methods to develop the ionizable cationic lipids for mRNA delivery, not on mRNA optimization itself. We did, however, perform comparison studies, concentrating on characterizing the luciferase expression *in vitro* and *in vivo* by delivering luciferase mRNA by AA3-DLin LNPs, ALC-0315 LNPs (Pfizer/BioNTech), and MC3 LNPs. Additionally, for vaccine comparison studies, we evaluated the spike-specific antibody IgG titers, pseudovirus neutralization and $PRNT_{50}$ by delivering wild-type spike mRNA using FDA-approved LNP formulations. Second, in future studies, the lyophilized mRNA-LNP formulations should be optimized for long-term storage at even higher temperatures, especially in 4 °C or RT. These improvements will enhance the storage capability of not only COVID-19 vaccines but also future mRNA therapeutics and drugs.

CONCLUSIONS

In summary, this study reports a one-step chemical-biological CALB enzyme-catalyzed synthesis for high-throughput development of a series of ionizable cationic lipids for the mRNA-LNP delivery platforms. Increasing the phospholipid proportion in LNP formulations extensively enhances the mRNA delivery eficacy which may guide the optimization of mRNA-LNP delivery platforms for future studies. The transfection and COVID-19 vaccine studies performed have proven the potential of AA3-DLin LNPs to be an effective and robust mRNA delivery platform with excellent long-term storage capability without ultracold conditions, lending itself to adaption for limitless uses in mRNA delivery applications. More importantly, this work exhibits a comprehensive bottom-up methodology to evaluate the developed ionizable cationic lipids, incorporating lipid design, synthesis, screening, optimization, fabrication, characterization as well as *in vitro* and *in vivo* applications. We expect this CALB enzyme-catalyzed chemical synthesis methodology to provide overall perspectives for synthesizing ionizable cationic lipids, expanding the field of lipid-like materials, and paving an avenue for next-generation genetic therapy.

EXPERIMENTAL SECTION

Ionizable Cationic Lipid Library Synthesis. A CALB enzyme-catalyzed esterification was utilized to synthesize ionizable cationic lipids between hydroxyl groups (−OH) of amino alcohol and carboxylic acid groups (−COOH) of lipid acids.[23,24] Briefly, amino alcohol was dissolved in THF using two-neck round-bottom flask, and then 0.5 g of amino alcohol was added and dissolved in 5 mL of THF followed by the addition of 2 molar ratio excess of lipid acid and 0.5 g of CALB. The reaction lasted for 72 h with the protection of nitrogen at 60 °C. Then, the CALB was removed by centrifuge, and the supernatant was collected and purified by saturated $NaHCO_3$ solution to neutralize the excess lipid acid. Then the resultant was extracted by excess ethyl acetate following drying with anhydrous $MgSO_4$. A clear lipid ethyl acetate solution was obtained after removing $MgSO_4$ by centrifuge and the lipid solution was concentrated by rotatory evaporating to remove the ethyl acetate and the resulting lipids were dried in vacuum for 48 h until use. The purified lipid product was characterized by ^1H NMR spectrometry (500 MHz, Bruker spectrometer) and High Resolution Orbitrap Q Exactive LC/MS spectrometry (Thermo Fisher Scientific), and the Nicolet IS-10 spectrometer was used to collected FTIR spectra (Thermo Fisher Scientific).

High-Throughput Screening of Ionizable Cationic Lipid Library *in Vitro*. The lipid-like materials were synthesized through a CALB enzyme-catalyzed reaction between the amino alcohols (AA) and lipid acids. The lipids were named in the form of "AA#-lipid". In all cases, "#" indicates the number of amino alcohols as shown in Amino Alcohol Library, "lipid" indicates the different lipids in Lipid Acid Library. In the preliminary screening of the lipid library, the ionizable lipids, DOPE, DMG-PEG, and cholesterol were dissolved in ethanol with the concentration of 10 mg/mL, and the luciferase mRNAs (mLuc) were dissolved by NaOAc buffer (25 mM, pH 5.0). The mLuc loaded LNPs were formulated via pipetting the mRNA NaOAc solution to lipid ethanol mixtures with a 1:3 volume ratio (ethanol: NaOAc, v./v.) followed by 20 min of incubation at RT before experiments with a widely used LNP formulation of 50:10:38.5:1.5 and a fixed weight ratio of 1:20 (mRNA: ionizable lipid, wt./wt.). These different mLuc (0.1 μg) loaded LNPs were used to transfect Hek 293 cells. The mRNA-LNP transfection eficacy was determined by the luciferase expression intensity, which was analyzed by Bright-Glo luciferase assay, and the luciferase intensity was recorded by Tecan plate reader (Tecan Infinite M200 Pro) after 24 h incubation.

Orthogonal Design of Experiment for Optimizing LNP Formulation. An orthogonal design of experiment (DoE) methodology was carried out to screen the optimized molar ratio of lipids in the AA3-DLin LNPs. Different AA3-DLin LNP formulations were prepared in accordance with details in two orthogonal design tables L16 (4^4) termed library A and library B and use mLuc as a reporter gene. These mLuc (0.1 μg) loaded LNP formulations were used to transfect Hek 293 cells seeded in a 96-well plate, and the transfection eficacy was measured by Bright-Glo luciferase assay and recorded by a plate reader after 24 h post-transfection.

The MC3 LNPs were prepared as MC3/DSPC/cholesterol/DMG-PEG = 50:10:38.5:1.5 and the ALC-0315 LNPs were formulated with ALC-0315/DSPC/cholesterol/DMG-PEG at molar ratio of 46/10/42/2. All the LNPs were used with the same manner as described above to transfect cells. Lipofectamine 3000 was applied corresponding to the instructions. Additionally, the cytotoxicity was evaluated using CCK-8 assay, and the cell viability results were normalized to the value of the control group.

Fabrication of mRNA Loaded LNPs by Microfluidic Chip Device. A microfluidic-chip device was employed to fabricate the LNPs with uniform particle size. The microfluidic chip device used for AA3-DLin LNP fabrication was reported in a previous study.[37] The ethanol phase contained a mixture of AA3-DLin, DOPE, cholesterol, and DMG-PEG with an optimized 40:40:25:0.5 molar ratio. Either luciferase encoded mRNA (mLuc), mCherry encoded mRNA (mCherry), or antigen full-length spike encoded mRNA (mspike) was dissolved in 25 mM NaOAc buffer (pH 5.0) to compose the aqueous phase. The aqueous and ethanol organic phases were loaded in two different syringes at a volume ratio of 1:3 and a fixed mRNA/AA3-DLin weight ratio of 1:20 for *in vitro* and 1:10 for *in vivo*, respectively. The two phases were mixed by syringe pumps to quickly flow through a microfluidic chip device with preset pump rates. The resulting LNPs were subsequently incubated for 20 min at RT before dialysis against 1× PBS in a dialysis tube (MWCO 3.5 kDa) for 2 h at RT to remove ethanol. The fresh LNPs could be concentrated or diluted on demand or used directly for studies. For the long-term storage studies of AA3-DLin LNPs, different concentrations of sucrose solution were added and mixed thoroughly with the fresh LNPs. A freeze-drying process was carried out for the lyophilized LNP groups. Then the lyophilized LNP powders or LNP formulations were stored at either 4 °C or −20 °C for 12 months. The lyophilized LNP powders were resuspended thoroughly in 25 mM pH 5.0 NaOAc buffer, and the frozen LNP were thawed at RT before experiments.

LNP Characterizations and Morphology Analysis. The zeta potentials, PDI and particle size were characterized in DI water by a Dynamic Light Scattering and Zeta Potential Detector (Malvern, UK). The intensity-weighted mean values were displayed as mean ± SD after measurements in tripicate.[58]

https://doi.org/10.1021/acsnano.2c07822
ACS Nano 2022, 16, 18936−18950

Quant-iT RiboGreen RNA Assay Kit (Invitrogen) was used to characterize mRNA encapsulation eficiency. Briefly, the mRNA-loaded AA3-DLin LNP solution was incubated with Ribogreen, and the fluorescence intensity was measured to obtain the unencapsulated mRNA. Then, 2% Triton X-100 was added to the AA3-DLin LNP solution for 10 min allowing mRNA release by breaking apart the particles, the fluorescence intensity was measured after incubating with Ribogreen as total mRNA.[36,37,59,60] The mRNA encapsulation eficiency (%) was calculated by

$$\text{mRNA (encapsulation efficiency\%)} = \frac{(\text{total mRNA} - \text{free mRNA})}{\text{total mRNA}} \times 100\%$$

The acid dissociation constant (pK_a) was measured by TNS as reported before.[7,28,59] Briefly, the mRNA-loaded AA3-DLin LNP formulation was added to a series of buffers containing 10 mM MES, 130 mM NaCl, 10 mM HEPES, and 10 mM ammonium, with the pH values ranging from 3.0 to 11.0. 100 μM TNS was prepared as a stock solution and incubated with the above solution for 5 min with slight shaking. The total volume of each sample was 100 μL in a 96-well plate with 50 μM total lipids and 5 μM TNS in the final concentration. The fluorescence intensity was recorded at 321 nm excitation wavelengths and 445 nm emission wavelengths by a plate reader (Tecan). The fluorescence intensity was normalized to the value of pH 3.0, and the pH value at half-maximal fluorescence intensity was determined to be the pK_a.

Agarose gel electrophoresis assay was conducted to investigate the binding eficiency of mRNA-loaded AA3-DLin LNPs. 2uL of RNA loading dye was added into 10 uL of LNP samples, and then the mixtures were loaded on the gel and run for half an hour.

The morphology of AA3-DLin LNPs were evaluated using a transmission electron microscope (TEM, JEM-F200). Five μL of AA3-DLin LNP was dropped on the TEM copper grid and blotted away with Kimwipes after 1 min. Then 5 μL of uranyl acetate solution (2%) was used to stain the LNP samples for half-minute, followed by blotting away the staining solution by a filter paper. The staining process was repeated for a total of three times in the same manner and the LNP sample was allowed to be air-dried in the fume hood.

Antigen Encoded mRNA Synthesis. An *in vitro* transcription (IVT) process was used to synthesize the wild-type SARS-CoV-2 spike mRNA with regular nucleosides. A 5′ untranslated region (UTR) with a Kozak translational initiation signal and an alpha-globin 3′ UTR terminating sequence were flanked into the open reading frame of spike protein with the addition of a polyA tail at the end. An Anti-Reverse Cap Analog (ARCA) was capped for the IVT mRNA synthesis.

Cells and Animals. Hek 293 cells were received from ATCC. The ACE2-293T cells were kindly obtained from Dr. Dongfang Liu from NJMS. The splenocytes were harvested from vaccinated mice. Generally, 293 cells were cultured in DMEM, and the splenocytes were cultured with RPMI 1640, both media were supplied with 10% FBS and 1% penicillin−streptomycin. The mice used for experiments were obtained from the Jackson Laboratory. Animal experimental protocols including ethical compliance were approved by the Animal Care and Use Committee (eIACUC) at Rutgers-NJMS, where mice were housed.

Evaluation of LNP Transfection Eficacy *in Vitro*. The transfection eficacy of LNPs *in vitro* was also characterized by delivering mCherry mRNA into Hek 293 cells. Briefly, 1×10^5 cells were seeded into a 24-well plate for overnight incubation. The second day, fresh mCherry-LNPs or the stored mCherry-LNPs were directly added into the cell medium with a fixed amount of 1 μg mCherry per well. Images of transfected mCherry positive cells were captured by a fluorescence microscope (BZ-X710, Keyence) at predetermined time points. After the cells were imaged, they were harvested by Trypsin-EDTA, and suspended in PBS to obtain the cell pellets after centrifugation. Then, a BD LSR II flow cytometer and FACSDiva software (BD Biosciences, U.S.A.) were used to analyze the collected cells. The mCherry positive cells were detected by a 561 nm laser with a 610/20 BP filter at 350 V. Overall, 10 000 events per sample were recorded.

Bioluminescence Study *in Vivo*. Bioluminescence imaging studies were carried out using BALB/c mice (6−8 weeks, female, 18−20 g). Briefly, 100 μL of fresh luciferase mRNA (10 μg mRNA, 0.5 mg/kg) was loaded into AA3-DLin LNPs (n = 3) and injected intramuscularly at the hind leg. Luciferase mRNA (10 μg) diluted in 90 μL of PBS was injected into mice as control groups (n = 3). For AA3-DLin LNP long-term storage studies, lyophilized luciferase mRNA-encapsulating LNPs (10 μg mRNA, 0.5 mg/kg) (n = 3) (with 10 wt % sucrose) were resuspended in 100 μL of NaOAc buffer, and the frozen luciferase mRNA-encapsulating LNPs (10 μg mRNA, 0.5 mg/kg) (n = 3) (with 5 wt % sucrose) were thawed at RT before mouse injections in the same manner. For stability studies, AA3-DLin LNPs (n = 3) formulated with 5 wt % sucrose were stored at either 4 or 25 °C for 1, 3, 5, 7, and 9 days before being injected into mice. At a preset timeline, 150 μL of D-Luciferin potassium salt solution (30 mg/mL) was injected intraperitoneally into mice. The bioluminescence images were captured by IVIS spectrum instrument (Xenogen) within 20 min post-injection, and the exposure time was set to 30 s. Bioluminescence intensity was quantified by characterizing the total photon flux in the region of interest.

Western Blot. Hek 293 cells transfected by 1 μg spike mRNA loaded AA3-DLin LNPs in a 24-well plate were lysed by cold lysis buffer. After the protein concentration was measured, loading dye was added to each lysed sample following 5 min of boiling. In the meantime, a 12% resolving, 5% stacking SDS-PAGE gel was prepared. Then, a polyvinylidene difluoride (PVDF) membrane was used to transfer protein followed by blocking in 3% BSA PBS solution overnight. The next day, the membrane was probed using rabbit anti-spike (1:1000) and rabbit anti-GAPDH (1:2000) antibodies for 2 h. Tris-buffered saline Tween 20 (TBST) was used to wash the membrane three times, and then HRP conjugated anti-rabbit antibody (1:5000) was applied to the membrane for 1 h at RT. Lastly, chemiluminescence substrate (PerkinElmer) was used to visualize the proteins on the membrane after three washes in TBST.

Immunofluorescence Assay. An immunofluorescence assay was carried out to stain the AA3-DLin LNP (1 μg spike mRNA loaded) transfected cells. In brief, 2×10^5 Hek 293 cells were seeded in a 12-well plate in which cover glasses were placed in each well. The second day, AA3-DLin LNPs were added to transfect the cells for 48 h. Then, the cells were fixed using paraformaldehyde (4%, PFA) solution and methanol for 10 min, respectively, followed by washes with PBS. The fixed cells were incubated with 3% BSA for 30 min. Next, rabbit anti-spike (1:500) was added to the cells for 2 h at RT. After the cells were washed three times, goat Alexa Fluor 488 anti-rabbit IgG (1:1000) was used to stain the cells for 1 h at RT. After three additional washes, DAPI (Invitrogen) was applied to the cells for nuclear staining. The slides were sealed, and the cell were imaged by a fluorescence microscope.

Tissue Immunofluorescence Assay and Histology. AA3-DLin LNP treated mice were sacrificed after bioluminescence imaging, and the muscle tissue of the administration sites were harvested and submerged in 4% PFA overnight, followed by tissue dehydration with 30% sucrose solution. Tissue samples were put into cryomolds, embedded with O.C.T. compound and kept frozen. The tissue samples were sectioned using a cryostat (15 μm thickness). For tissue immunofluorescence assay, tissue sections were blocked using 5% goat serum and 3% BSA for 1 h at RT and then permeabilized by 1% TritonX-100 solution for half an hour. Then, the samples were probed with rabbit anti-IL-6 (1:1000) overnight. The second day, after three washes, tissue samples were incubated with Alexa Fluor 488 goat anti-rabbit IgG (1:1000) for 2 h. After another three washes, the slides were mounted and covered by coverslips. For histology experiments, hematoxylin and eosin (H&E) staining was used for tissue histopathological examination.

Mouse Vaccination Study. Five BALB/c mice per group (6−8 weeks, female) were used for vaccination experiments. Doses of 2 μg or 10 μg spike mRNA-loaded AA3-DLin vaccines (with 5 wt % sucrose) after 12-month frozen storage at −20 °C, and fresh AA3-

https://doi.org/10.1021/acsnano.2c07822
ACS Nano 2022, 16, 18936−18950

DLin vaccines were intramuscularly administered in the left hind leg for all vaccination studies. For the placebo group, 100 μL of empty AA3-DLin LNPs was injected in the same manner.[55] The mouse blood was collected from the orbital sinus, and spleens were harvested on day 30 for T cell immune response analysis. The blood samples were centrifuged at 3000*g*, and the collected sera were heat-inactivated for 30 min at 56 °C.

SARS-CoV-2 ELISA Assay. ELISA kits were used to determine SARS-CoV-2 spike-specific antibody titers of the immunized mice. In brief, 96-well ELISA plates (MaxiSorp) were coated with 0.1 μg SARS-CoV-2 spike protein (Sino Biological) for each well and put in 4 °C overnight. The second day, 200 μL wash buffer (Thermo Fisher Scientific) was used to wash each well three times, followed by blocking with 200 μL assay buffer at RT for 1 h. 100 μL of serial diluted sera samples was put into protein-coated plates for 2 h. The plates were washed in triplicate, and then 50 μL of HRP goat anti-mouse IgG (1:3000) was added for a 1 h incubation at RT followed by three washes. Next, 50 μL of TMB substrate solution per well was applied to detect the binding antibody followed by 50 μL of stop solution. A Tecan plate reader was used to detect the absorbance signal at 450 nm. The endpoint titers were determined to be the highest reciprocal serum dilution, yielding more than 2.1 fold of absorbance over control.[61,62]

Plaque Reduction Neutralization Test. PRNT was performed to investigate the AA3-DLin vaccine immunogenicity against real virus. Briefly, the serial diluted sera were cultured with 200 PFU/mL of wild-type SARS-CoV-2 virus for 1 h at 37 °C. The sera−virus mixture samples were placed in 24-well plates seeded with the Vero cell monolayers for 1 h at 37 °C with intermittent shaking. The media was then replaced with DMEM (supplied with 2% FBS and 1% agarose). Cells were further incubated for another 2 days followed by fixation with 4% PFA, then the cell samples were incubated with 0.2% crystal violet. The plaque numbers were counted after rinsing with DI water. The 50% plaque reduction neutralization test ($PRNT_{50}$) was analyzed and recorded.[61]

SARS-CoV-2 Pseudovirus Neutralization Assay. The luciferase expressed SARS-CoV-2 pseudovirus (Creative Biogene, Inc.) was incubated with serial diluted serum samples at 37 °C for 1 h, before adding to ACE2-293T cells seeded in 96-well microplates. Luciferase activity was recorded by a Tecan plate reader using Bright-Glo Luciferase Assay after 48 h post-infection and the luciferase intensity was normalized as relative light units (RLU). Neutralization IC50 titers were defined as the serum dilution showing 50% RLU reduction with respect to the RLU of pseudovirus-only minus background.

ELISpot. For the ELISpot study, the splenocytes were collected individually from the vaccinated mice groups. Briefly, the spleens were homogenized and filtrated by a 70 μm strainer followed by addition of ACK lysis buffer and then the collected splenocytes were cultured in complete RPMI1640 media. Mouse IFN-γ ELISpot kit (Mabtech) was utilized to evaluate SARS-CoV-2 T cell responses. The cell plates were then washed in triplicate followed by blocking for 2 h in RPMI1640. Then 2×10^5 of splenocytes were transferred to the cell plates and then activated with the peptide pool (2 μg/mL, Miltenyi Biotec) at 37 °C for 24 h. After the cells were washed three times, the cells were probed with a detection antibody (biotin-conjugated) for 2 h, and washed again thrice. Then streptavidin-ALP was added for 1 h, and another three plate washes were performed before the plates were incubated for 20 min with BCIP/NBT. At last, DI water was applied to stop the color reaction and the plates were dried in darkness. CTL ImmunoSpot Analyzer was used to image and analyze the dark spots.

Intracellular Cytokine Staining. The intracellular cytokine staining studies were carried out to characterize the cytokine-producing T cells. Briefly, 1×10^6 of splenocytes were cultured in a 96-well plate and activated by the peptide pool (2 μg/mL) for 6 h with the addition of BD GolgiPlug at 37 °C. Cells were treated with LIVE/DEAD Cell Stain Kit (Fixable Near-IR, 1:1000, Invitrogen) after three washes. Then, antibodies of cell surface markers including anti-CD3 (1:100), anti-CD8a (1:100) and anti-CD4 (1:100) were added to the stimulated splenocytes. After being washed, the splenocytes were treated with BD Cytofix/Cytoperm, and washed by Perm/Wash buffer. Splenocytes were incubated with a mixture of intracellular cytokine marker antibodies including anti-IFN-γ (1:100), anti-IL-2 (1:100), anti-TNF (1:100), and anti-IL-4 (1:100). After the cells were stained, flow cytometric analysis was performed, and the results were collected using FACS Diva software BD (100,000 events collected).

Statistical Analysis. GraphPad Prism 8 software was used to analyze the statistical significance. Unpaired *t* test and one-way ANOVA were applied to compare two groups and multiple groups, respectively. Statistical significance was defined as $p < 0.05$ (ns, not significant; *$p < 0.05$, **$p < 0.01$, ***$p < 0.001$, ****$p < 0.0001$).

ASSOCIATED CONTENT

* Supporting Information

The Supporting Information is available free of charge at https://pubs.acs.org/doi/10.1021/acsnano.2c07822.

Includes Materials, Figures S1−S11, Tables S1−S8. Figure S1: The mechanism of CALB enzyme-assisted esterification. Figures S2−S9: The additional characterizations of ionizable cationic lipids and lipid nanoparticles. Figure S10: amino acid sequence of spike protein used in vaccination studies. Figure S11: flow cytometry gating strategy of intracellular cytokine staining. Table S1: Characterization of lipid-like materials. Table S2−S7: Characterization and detailed formulations of different AA3-DLin LNPs. Table S8: the list of antibodies used in this study (PDF)

AUTHOR INFORMATION

Corresponding Authors

Xue-Qing Zhang − *Engineering Research Center of Cell & Therapeutic Antibody Ministry of Education, School of Pharmacy, Shanghai Jiao Tong University, Shanghai 200240, P. R. China;* orcid.org/0000-0002-4954-2586; Email: xueqingzhang@sjtu.edu.cn

Xiaoyang Xu − *Department of Chemical and Materials Engineering, New Jersey Institute of Technology, Newark, New Jersey 07102, United States; Department of Biomedical Engineering, New Jersey Institute of Technology, Newark, New Jersey 07102, United States;* orcid.org/0000-0002-1634-3329; Email: xiaoyang.xu@njit.edu

Authors

Zhongyu Li − *Department of Chemical and Materials Engineering, New Jersey Institute of Technology, Newark, New Jersey 07102, United States;* orcid.org/0000-0002-9566-5771

William Ho − *Department of Chemical and Materials Engineering, New Jersey Institute of Technology, Newark, New Jersey 07102, United States*

Fengqiao Li − *Department of Chemical and Materials Engineering, New Jersey Institute of Technology, Newark, New Jersey 07102, United States*

Mingzhu Gao − *Engineering Research Center of Cell & Therapeutic Antibody Ministry of Education, School of Pharmacy, Shanghai Jiao Tong University, Shanghai 200240, P. R. China*

Xin Bai − *Engineering Research Center of Cell & Therapeutic Antibody Ministry of Education, School of Pharmacy, Shanghai Jiao Tong University, Shanghai 200240, P. R. China*

Complete contact information is available at: https://pubs.acs.org/10.1021/acsnano.2c07822

Author Contributions

Z.L. and X.X. initiated this project. Z.L. designed, synthesized the materials, fabricated LNPs, and carried out most of the *in vitro* and *in vivo* experiments. Z.L., W.H., F.L., M.G., X.B., X.Z., and X.X. discussed the results and reviewed the conclusions. Z.L. and X.X. wrote the manuscript. Z.L., W.H., X.Z., and X.X. edited and reviewed the manuscript. Z.L. and X.Z. contributed equally. Z.L., X.Z., and X.X. were mainly responsible for data interpretation.

Notes

The authors declare no competing financial interest.

ACKNOWLEDGMENTS

X.X. acknowledges funding from National Science Foundation (2001606) and American Heart Association grant #19AIREA34380849. This research is also supported by the Gustavus and Louise Pfeiffer Research Foundation Award. X.-Q.Z. recognizes funding from the Foundation of National Facility for Translational Medicine (Shanghai) (TMSK-2020-008) and Shanghai Jiao Tong University Scientific and Technological Innovation Funds (2019TPA10) and the Interdisciplinary Program of Shanghai Jiao Tong University [ZH2018ZDA36 (19 × 190020006)].

REFERENCES

(1) Sahin, U.; Muik, A.; Derhovanessian, E.; Vogler, I.; Kranz, L. M.; Vormehr, M.; Baum, A.; Pascal, K.; Quandt, J.; Maurus, D.; et al. COVID-19 vaccine BNT162b1 elicits human antibody and TH 1 T cell responses. *Nature* 2020, *586* (7830), 594−599.

(2) Baden, L. R.; El Sahly, H. M.; Essink, B.; Kotloff, K.; Frey, S.; Novak, R.; Diemert, D.; Spector, S. A.; Rouphael, N.; Creech, C. B.; et al. Efficacy and safety of the mRNA-1273 SARS-CoV-2 vaccine. *New England Journal of Medicine* 2021, *384* (5), 403−416.

(3) Ho, W.; Gao, M.; Li, F.; Li, Z.; Zhang, X. Q.; Xu, X. Next-Generation Vaccines: Nanoparticle-Mediated DNA and mRNA Delivery. *Adv. Healthcare Mater.* 2021, *10* (8), 2001812.

(4) Cullis, P. R.; Hope, M. J. Lipid nanoparticle systems for enabling gene therapies. *Molecular Therapy* 2017, *25* (7), 1467−1475.

(5) Hou, X.; Zaks, T.; Langer, R.; Dong, Y. Lipid nanoparticles for mRNA delivery. *Nat. Rev. Mater.* 2021, *6*, 1078−1094.

(6) Chaudhary, N.; Weissman, D.; Whitehead, K. A. mRNA vaccines for infectious diseases: principles, delivery and clinical translation. *Nat. Rev. Drug Discovery* 2021, *20*, 817−838.

(7) Jayaraman, M.; Ansell, S. M.; Mui, B. L.; Tam, Y. K.; Chen, J.; Du, X.; Butler, D.; Eltepu, L.; Matsuda, S.; Narayanannair, J. K.; et al. Maximizing the potency of siRNA lipid nanoparticles for hepatic gene silencing in vivo. *Angew. Chem.* 2012, *124* (34), 8657−8661.

(8) Semple, S. C.; Akinc, A.; Chen, J.; Sandhu, A. P.; Mui, B. L.; Cho, C. K.; Sah, D. W.; Stebbing, D.; Crosley, E. J.; Yaworski, E. Rational design of cationic lipids for siRNA delivery. *Nature biotechnology* 2010, *28* (2), 172−176.

(9) Miao, L.; Zhang, Y.; Huang, L. mRNA vaccine for cancer immunotherapy. *Mol. Cancer* 2021, *20* (1), 1−23.

(10) Cheng, X.; Lee, R. J. The role of helper lipids in lipid nanoparticles (LNPs) designed for oligonucleotide delivery. *Advanced drug delivery reviews* 2016, *99*, 129−137.

(11) Buschmann, M. D.; Carrasco, M. J.; Alishetty, S.; Paige, M.; Alameh, M. G.; Weissman, D. Nanomaterial delivery systems for mRNA vaccines. *Vaccines* 2021, *9* (1), 65.

(12) Qiu, M.; Glass, Z.; Chen, J.; Haas, M.; Jin, X.; Zhao, X.; Rui, X.; Ye, Z.; Li, Y.; Zhang, F.; Xu, Q. Lipid nanoparticle-mediated codelivery of Cas9 mRNA and single-guide RNA achieves liver-specific in vivo genome editing of Angptl3. *Proc. Natl. Acad. Sci. U. S. A.* 2021, *118*, e2020401118.

(13) Musunuru, K.; Chadwick, A. C.; Mizoguchi, T.; Garcia, S. P.; DeNizio, J. E.; Reiss, C. W.; Wang, K.; Iyer, S.; Dutta, C.; Clendaniel, V.; et al. In vivo CRISPR base editing of PCSK9 durably lowers cholesterol in primates. *Nature* 2021, *593* (7859), 429−434.

(14) Gillmore, J. D.; Gane, E.; Taubel, J.; Kao, J.; Fontana, M.; Maitland, M. L.; Seitzer, J.; O'Connell, D.; Walsh, K. R.; Wood, K.; et al. CRISPR-Cas9 in vivo gene editing for transthyretin amyloidosis. *New England Journal of Medicine* 2021, *385* (6), 493−502.

(15) Lin, Y.-X.; Wang, Y.; Ding, J.; Jiang, A.; Wang, J.; Yu, M.; Blake, S.; Liu, S.; Bieberich, C. J.; Farokhzad, O. C.; et al. Reactivation of the tumor suppressor PTEN by mRNA nanoparticles enhances antitumor immunity in preclinical models. *Science Translational Medicine* 2021, *13*, 599.

(16) Hotz, C.; Wagenaar, T. R.; Gieseke, F.; Bangari, D. S.; Callahan, M.; Cao, H.; Diekmann, J.; Diken, M.; Grunwitz, C.; Hebert, A.; et al. Local delivery of mRNA-encoded cytokines promotes antitumor immunity and tumor eradication across multiple preclinical tumor models. *Science Translational Medicine* 2021, *13* (610), eabc7804.

(17) Ansell, S. M.; Du, X.Novel lipids and lipid nanoparticle formulations for delivery of nucleic acids. U.S. Patent Application No. 17/317,517. Oct. 28, 2015.

(18) Sabnis, S.; Kumarasinghe, E. S.; Salerno, T.; Mihai, C.; Ketova, T.; Senn, J. J.; Lynn, A.; Bulychev, A.; McFadyen, I.; Chan, J.; et al. A novel amino lipid series for mRNA delivery: improved endosomal escape and sustained pharmacology and safety in non-human primates. *Molecular Therapy* 2018, *26* (6), 1509−1519.

(19) Xu, X.; Xie, K.; Zhang, X.-Q.; Pridgen, E. M.; Park, G. Y.; Cui, D. S.; Shi, J.; Wu, J.; Kantoff, P. W.; Lippard, S. J.; et al. Enhancing tumor cell response to chemotherapy through nanoparticle-mediated codelivery of siRNA and cisplatin prodrug. *Proc. Natl. Acad. Sci. U. S. A.* 2013, *110* (46), 18638−18643.

(20) Love, K. T.; Mahon, K. P.; Levins, C. G.; Whitehead, K. A.; Querbes, W.; Dorkin, J. R.; Qin, J.; Cantley, W.; Qin, L. L.; Racie, T.; et al. Lipid-like materials for low-dose, in vivo gene silencing. *Proc. Natl. Acad. Sci. U. S. A.* 2010, *107* (5), 1864−1869.

(21) Dong, Y.; Love, K. T.; Dorkin, J. R.; Sirirungruang, S.; Zhang, Y.; Chen, D.; Bogorad, R. L.; Yin, H.; Chen, Y.; Vegas, A. J.; et al. Lipopeptide nanoparticles for potent and selective siRNA delivery in rodents and nonhuman primates. *Proc. Natl. Acad. Sci. U. S. A.* 2014, *111* (11), 3955−3960.

(22) Li, B.; Luo, X.; Deng, B.; Wang, J.; McComb, D. W.; Shi, Y.; Gaensler, K. M. L.; Tan, X.; Dunn, A. L.; Kerlin, B. A.; Dong, Y. An orthogonal array optimization of lipid-like nanoparticles for mRNA delivery in vivo. *Nano Lett.* 2015, *15* (12), 8099−8107.

(23) Li, Z.; Zhang, X.-Q.; Ho, W.; Bai, X.; Jaijyan, D. K.; Li, F.; Kumar, R.; Kolloli, A.; Subbian, S.; Zhu, H.; Xu, X. Lipid-Polymer Hybrid "Particle-in-Particle" Nanostructure Gene Delivery Platform Explored for Lyophilizable DNA and mRNA COVID-19 Vaccines. *Adv. Funct. Mater.* 2022, *32*, 2204462.

(24) Tsou, Y. H.; Zhang, X. Q.; Bai, X.; Zhu, H.; Li, Z.; Liu, Y.; Shi, J.; Xu, X. Dopant-Free Hydrogels with Intrinsic Photoluminescence and Biodegradable Properties. *Adv. Funct. Mater.* 2018, *28* (34), 1802607.

(25) Ortiz, C.; Ferreira, M. L.; Barbosa, O.; dos Santos, J. C.; Rodrigues, R. C.; Berenguer-Murcia, A.; Briand, L. E.; Fernandez-Lafuente, R. Novozym 435: the "perfect" lipase immobilized biocatalyst? *Catalysis Science & Technology* 2019, *9* (10), 2380−2420.

(26) Basso, A.; Serban, S. Industrial applications of immobilized enzymes—A review. *Molecular Catalysis* 2019, *479*, 110607.

(27) Kundys, A.; Białecka-Florjanczyk, E.; Fabiszewska, A.; Małajowicz, J. Candida antarctica lipase B as catalyst for cyclic esters synthesis, their polymerization and degradation of aliphatic polyesters. *Journal of Polymers and the Environment* 2018, *26* (1), 396−407.

(28) Cheng, Q.; Wei, T.; Jia, Y.; Farbiak, L.; Zhou, K.; Zhang, S.; Wei, Y.; Zhu, H.; Siegwart, D. J. Dendrimer-based lipid nanoparticles deliver therapeutic FAH mRNA to normalize liver function and extend survival in a mouse model of hepatorenal tyrosinemia type I. *Advanced materials* 2018, *30* (52), 1805308.

(29) Schoenmaker, L.; Witzigmann, D.; Kulkarni, J. A.; Verbeke, R.; Kersten, G.; Jiskoot, W.; Crommelin, D. J. mRNA-lipid nanoparticle

https://doi.org/10.1021/acsnano.2c07822
ACS Nano 2022, 16, 18936−18950

COVID-19 vaccines: Structure and stability. *Int. J. Pharm.* 2021, *601*, 120586.
(30) Miao, L.; Li, L.; Huang, Y.; Delcassian, D.; Chahal, J.; Han, J.; Shi, Y.; Sadtler, K.; Gao, W.; Lin, J.; et al. Delivery of mRNA vaccines with heterocyclic lipids increases anti-tumor efficacy by STING-mediated immune cell activation. *Nature biotechnology* 2019, *37* (10), 1174−1185.
(31) Sen, S.; Puskas, J. E. Green polymer chemistry: Enzyme catalysis for polymer functionalization. *Molecules* 2015, *20* (5), 9358−9379.
(32) Jakovetic, S. M.; Jugovic, B. Z.; Gvozdenovic, M. M.; Bezbradica, D. I.; Antov, M. G.; Mijin, D. Z.; Knezevic-Jugovic, Z. D. Synthesis of aliphatic esters of cinnamic acid as potential lipophilic antioxidants catalyzed by lipase B from Candida antarctica. *Appl. Biochem. Biotechnol.* 2013, *170* (7), 1560−1573.
(33) Shinkai, S.; Araki, K.; Tsubaki, T.; Arimura, T.; Manabe, O. New syntheses of calixarene-p-sulphonates and p-nitrocalixarenes. *Journal of the Chemical Society, Perkin Transactions 1* 1987, 2297−2299.
(34) Kauffman, K. J.; Dorkin, J. R.; Yang, J. H.; Heartlein, M. W.; DeRosa, F.; Mir, F. F.; Fenton, O. S.; Anderson, D. G. Optimization of lipid nanoparticle formulations for mRNA delivery in vivo with fractional factorial and definitive screening designs. *Nano Lett.* 2015, *15* (11), 7300−7306.
(35) Terada, T.; Kulkarni, J. A.; Huynh, A.; Chen, S.; van der Meel, R.; Tam, Y. Y. C.; Cullis, P. R. Characterization of lipid nanoparticles containing ionizable cationic lipids using design-of-experiments approach. *Langmuir* 2021, *37* (3), 1120−1128.
(36) Hassett, K. J.; Higgins, J.; Woods, A.; Levy, B.; Xia, Y.; Hsiao, C. J.; Acosta, E.; Almarsson, O.; Moore, M. J.; Brito, L. A. Impact of lipid nanoparticle size on mRNA vaccine immunogenicity. *J. Controlled Release* 2021, *335*, 237−246.
(37) Chen, D.; Love, K. T.; Chen, Y.; Eltoukhy, A. A.; Kastrup, C.; Sahay, G.; Jeon, A.; Dong, Y.; Whitehead, K. A.; Anderson, D. G. Rapid discovery of potent siRNA-containing lipid nanoparticles enabled by controlled microfluidic formulation. *J. Am. Chem. Soc.* 2012, *134* (16), 6948−6951.
(38) Kulkarni, J. A.; Darjuan, M. M.; Mercer, J. E.; Chen, S.; Van Der Meel, R.; Thewalt, J. L.; Tam, Y. Y. C.; Cullis, P. R. On the formation and morphology of lipid nanoparticles containing ionizable cationic lipids and siRNA. *ACS Nano* 2018, *12* (5), 4787−4795.
(39) van der Meel, R.; Chen, S.; Zaifman, J.; Kulkarni, J. A.; Zhang, X. R. S.; Tam, Y. K.; Bally, M. B.; Schiffelers, R. M.; Ciufolini, M. A.; Cullis, P. R.; Tam, Y. Y. C. Modular lipid nanoparticle platform technology for siRNA and lipophilic prodrug delivery. *Small* 2021, *17* (37), 2103025.
(40) Henrickson, A.; Kulkarni, J. A.; Zaifman, J.; Gorbet, G. E.; Cullis, P. R.; Demeler, B. Density matching multi-wavelength analytical ultracentrifugation to measure drug loading of lipid nanoparticle formulations. *ACS Nano* 2021, *15* (3), 5068−5076.
(41) Kamanzi, A.; Gu, Y.; Tahvildari, R.; Friedenberger, Z.; Zhu, X.; Berti, R.; Kurylowicz, M.; Witzigmann, D.; Kulkarni, J. A.; Leung, J.; et al. Simultaneous, single-particle measurements of size and loading give insights into the structure of drug-delivery nanoparticles. *ACS Nano* 2021, *15* (12), 19244−19255.
(42) Whitehead, K. A.; Dorkin, J. R.; Vegas, A. J.; Chang, P. H.; Veiseh, O.; Matthews, J.; Fenton, O. S.; Zhang, Y.; Olejnik, K. T.; Yesilyurt, V.; et al. Degradable lipid nanoparticles with predictable in vivo siRNA delivery activity. *Nat. Commun.* 2014, *5*, 4277.
(43) Zhao, P.; Hou, X.; Yan, J.; Du, S.; Xue, Y.; Li, W.; Xiang, G.; Dong, Y. Long-term storage of lipid-like nanoparticles for mRNA delivery. *Bioactive Materials* 2020, *5* (2), 358−363.
(44) Chen, C.; Han, D.; Cai, C.; Tang, X. An overview of liposome lyophilization and its future potential. *Journal of controlled release* 2010, *142* (3), 299−311.
(45) Stark, B.; Pabst, G.; Prassl, R. Long-term stability of sterically stabilized liposomes by freezing and freeze-drying: Effects of cryoprotectants on structure. *European journal of pharmaceutical sciences* 2010, *41* (3−4), 546−555.
(46) Heyes, J.; Palmer, L.; Bremner, K.; MacLachlan, I. Cationic lipid saturation influences intracellular delivery of encapsulated nucleic acids. *Journal of controlled release* 2005, *107* (2), 276−287.
(47) Tian, X.; Zhu, H.; Du, S.; Zhang, X.-Q.; Lin, F.; Ji, F.; Tsou, Y.-H.; Li, Z.; Feng, Y.; Ticehurst, K.; et al. Injectable PLGA-coated ropivacaine produces a long-lasting analgesic effect on incisional pain and neuropathic pain. *Journal of Pain* 2021, *22* (2), 180−195.
(48) Wang, B.; Tang, M.; Yuan, Z.; Li, Z.; Hu, B.; Bai, X.; Chu, J.; Xu, X.; Zhang, X.-Q. Targeted delivery of a STING agonist to brain tumors using bioengineered protein nanoparticles for enhanced immunotherapy. *Bioactive materials* 2022, *16*, 232−248.
(49) Bai, X.; Zhao, G.; Chen, Q.; Li, Z.; Gao, M.; Ho, W.; Xu, X.; Zhang, X.-Q. Inhaled siRNA nanoparticles targeting IL11 inhibit lung fibrosis and improve pulmonary function post-bleomycin challenge. *Sci. Adv.* 2022, *8* (25), eabn7162.
(50) Amanat, F.; Krammer, F. SARS-CoV-2 vaccines: status report. *Immunity* 2020, *52* (4), 583−589.
(51) Polack, F. P.; Thomas, S. J.; Kitchin, N.; Absalon, J.; Gurtman, A.; Lockhart, S.; Perez, J. L.; Pérez Marc, G.; Moreira, E. D.; Zerbini, C.; et al. Safety and efficacy of the BNT162b2 mRNA Covid-19 vaccine. *New England Journal of Medicine* 2020, *383* (27), 2603−2615.
(52) Lonez, C.; Vandenbranden, M.; Ruysschaert, J.-M. Cationic lipids activate intracellular signaling pathways. *Advanced drug delivery reviews* 2012, *64* (15), 1749−1758.
(53) Deng, L.; Wang, X.; Nie, K.; Wang, F.; Liu, J.; Wang, P.; Tan, T. Synthesis of wax esters by lipase-catalyzed esterification with immobilized lipase from Candida sp. 99−125. *Chinese Journal of Chemical Engineering* 2011, *19* (6), 978−982.
(54) Peng, X.; Ren, J.; Zhong, L.; Sun, R.; Shi, W.; Hu, B. Glycidyl methacrylate derivatized xylan-rich hemicelluloses: synthesis and characterizations. *Cellulose* 2012, *19* (4), 1361−1372.
(55) Corbett, K. S.; Edwards, D. K.; Leist, S. R.; Abiona, O. M.; Boyoglu-Barnum, S.; Gillespie, R. A.; Himansu, S.; Schäfer, A.; Ziwawo, C. T.; DiPiazza, A. T.; et al. SARS-CoV-2 mRNA vaccine design enabled by prototype pathogen preparedness. *Nature* 2020, *586* (7830), 567−571.
(56) Hsieh, C.-L.; Goldsmith, J. A.; Schaub, J. M.; DiVenere, A. M.; Kuo, H.-C.; Javanmardi, K.; Le, K. C.; Wrapp, D.; Lee, A. G.; Liu, Y.; et al. Structure-based design of prefusion-stabilized SARS-CoV-2 spikes. *Science* 2020, *369* (6510), 1501−1505.
(57) Vogel, A. B.; Kanevsky, I.; Che, Y.; Swanson, K. A.; Muik, A.; Vormehr, M.; Kranz, L. M.; Walzer, K. C.; Hein, S.; Guler, A.; et al. BNT162b vaccines protect rhesus macaques from SARS-CoV-2. *Nature* 2021, *592* (7853), 283−289.
(58) Li, Z.; Ho, W.; Bai, X.; Li, F.; Chen, Y.-j.; Zhang, X.-Q.; Xu, X. Nanoparticle depots for controlled and sustained gene delivery. *J. Controlled Release* 2020, *322*, 622−631.
(59) Chen, S.; Tam, Y. Y. C.; Lin, P. J.; Sung, M. M.; Tam, Y. K.; Cullis, P. R. Influence of particle size on the in vivo potency of lipid nanoparticle formulations of siRNA. *J. Controlled Release* 2016, *235*, 236−244.
(60) Chen, Q.; Gao, M.; Li, Z.; Xiao, Y.; Bai, X.; Boakye-Yiadom, K. O.; Xu, X.; Zhang, X.-Q. Biodegradable nanoparticles decorated with different carbohydrates for efficient macrophage-targeted gene therapy. *J. Controlled Release* 2020, *323*, 179−190.
(61) Zhang, N.-N.; Li, X.-F.; Deng, Y.-Q.; Zhao, H.; Huang, Y.-J.; Yang, G.; Huang, W.-J.; Gao, P.; Zhou, C.; Zhang, R.-R.; et al. A thermostable mRNA vaccine against COVID-19. *Cell* 2020, *182* (5), 1271.
(62) Wu, S.; Zhong, G.; Zhang, J.; Shuai, L.; Zhang, Z.; Wen, Z.; Wang, B.; Zhao, Z.; Song, X.; Chen, Y. A single dose of an adenovirus-vectored vaccine provides protection against SARS-CoV-2 challenge. *Nat. Commun.* 2020, *11*, 4081.

https://doi.org/10.1021/acsnano.2c07822
ACS Nano 2022, 16, 18936−18950